

Many-Objective Truss Structural Optimization Considering Dynamic and Stability Behaviors

João Marcos P. Vieira ^{1,†}, José Pedro G. Carvalho ², Dênis E. C. Vargas ³, Érica C. R. Carvalho ^{1,†},
Patrícia H. Hallak ⁴ and Afonso C. C. Lemonge ^{4,*}

- ¹ Graduate Program in Computational Modeling, Federal University of Juiz de Fora, Juiz de Fora 36036-900, Brazil; joaomarcos.vieira@estudante.ufjf.br (J.M.P.V.); erica.carvalho@estudante.ufjf.br (É.C.R.C.)
- ² Civil Engineering Program, COPPE/Federal University of Rio de Janeiro, Rio de Janeiro 21941-971, Brazil; jose.carvalho@coc.ufrj.br
- ³ Department of Mathematics, Federal Center for Technological Education of Minas Gerais, Belo Horizonte 30421-169, Brazil; denis.vargas@cefetmg.br
- ⁴ Department of Applied and Computational Mechanics, Federal University of Juiz de Fora, Juiz de Fora 36036-900, Brazil; patricia.hallak@ufjf.br
- * Correspondence: afonso.lemonge@ufjf.br
- † These authors contributed equally to this work.

Abstract: The most commonly used objective function in structural optimization is weight minimization. Nodal displacements, compliance, the first natural frequency of vibration, the critical load factor concerning global stability, and others can also be considered additional objective functions. This paper aims to propose seven innovative many-objective structural optimization problems (MOSOPs) applied to 25-, 56-, 72-, 120-, and 582-bar trusses, not yet presented in the literature, in which the main objectives, in addition to the structure's weight, refer to the structures' vibrational and stability aspects. These characteristics are essential in designing structural models, such as the natural frequencies of vibration and load factors concerning global stability. Such new MOSOPs have more than three objective functions and are called many-objective structural optimization problems. The chosen objective functions refer to the structure's weight, the natural frequencies of vibration, the difference between some of the natural frequencies of vibration, the critical load factor concerning the structure's global stability, and the difference between some of its load factors. The sizing design variables are the cross-sectional areas of the bars (continuous or discrete). The methodology involves the finite element method (FEM) to obtain the objective functions and constraints and multi-objective evolutionary algorithms (MOEAs) based on differential evolution to solve the MOSOPs analyzed in this study. In addition, multi-criteria decision-making (MCDM) is adopted to extract the solutions from the Pareto fronts according to the artificial decision-maker's (DM) preference scenarios, and the complete data for each chosen solution are provided. For the MOSOP with seven objective functions, it is possible to observe variations in the final weights of the optimum designs, considering the hypothetical scenarios, of 21.09% (25-bar truss), 289.73% (56-bar truss), 70.46% (72-bar truss), 45.35% (120-bar truss), and 74.92% (582-bar truss).

Keywords: many-objective structural optimization; differential evolution; multi-criteria decision-making; natural frequencies of vibration; global stability



Academic Editor: Christos Volos

Received: 12 December 2024

Revised: 5 January 2025

Accepted: 9 January 2025

Published: 14 January 2025

Citation: Vieira, J.M.P.; Carvalho, J.P.G.; Vargas, D.E.C.; Carvalho, É.C.R.; Hallak, P.H.; Lemonge, A.C.C.

Many-Objective Truss Structural Optimization Considering Dynamic and Stability Behaviors. *Dynamics* **2025**, *5*, 3. <https://doi.org/10.3390/dynamics5010003>

Copyright: © 2025 by the authors. Licensee MDPI, Basel, Switzerland.

This article is an open access article distributed under the terms and conditions of the Creative Commons Attribution (CC BY) license (<https://creativecommons.org/licenses/by/4.0/>).

1. Introduction

In a real-world structural optimization problem, a designer or decision-maker (DM) wants to find a structural configuration that satisfies the requirements imposed by a

standard or a usually recommended practice. Most of these optimization problems concern the structure's weight, mass, or total costs and use single-objective functions. On the other hand, multi-objective structural optimization problems (MOSOPs) can be formulated with the combination of several other conflicting objective functions. The most addressed MOSOPs concerning truss structures set only two objective functions: minimizing the weight and maximum nodal displacement, subjected to the allowable stresses on the bars. MOSOPs with more than three objective functions are called many-objective structural optimization problems.

In addition to weight and maximum nodal displacement, other objectives, such as natural frequencies of vibration, critical load factor, and compliance, may interest the designer when formulating structural optimization problems simultaneously. For example, studies presented by Carvalho et al. [1,2], which precede those presented in this paper, combined these objective functions in various formulations with two, three, and four objectives. In these studies, the importance of considering the natural frequencies of vibration and the critical load factors related to the global stability of the structure was emphasized, both of which must be maximized in conflict with the minimization of the structure's weight. For example, maximizing the first natural frequency of vibration prevents the possibility of resonance with low frequencies caused by dynamic loads, preventing the collapse of the structure. Similarly, maximizing the first critical load factor can ensure the structure's integrity, even if it is subjected to loads greater than those considered in its original designs.

The primary objective of this paper is to advance the field of structural optimization by introducing and addressing novel multi-objective structural optimization problems (MOSOPs) that have not yet been explored in the existing literature. These newly proposed MOSOPs integrate multiple objectives to provide a more comprehensive framework for structural design. Specifically, this study aims to simultaneously optimize several objective functions in addition to the structure's weight, including maximizing the first natural frequency of vibration and the first critical load factor, which are fundamental parameters for structural stability and dynamic behavior.

Furthermore, this paper introduces an innovative approach by incorporating the maximization of the differences between selected natural frequencies and critical load factors. This unique objective seeks to minimize the risk of mode superposition, which occurs when vibration or instability modes have closely spaced frequencies or load factors. Such superpositions can lead to resonance or compounded instabilities, significantly compromising structural integrity and safety. By maximizing these differences, the proposed framework enhances the robustness and reliability of the structure under dynamic and static loading conditions.

In total, seven novel MOSOPs are formulated in this study, encompassing four to seven distinct objective functions. This comprehensive formulation expands the scope of structural optimization by addressing a broader range of performance criteria. Additionally, this study emphasizes a balanced treatment of objectives and constraints. When natural frequencies or critical load factors are not considered as primary objectives, they are incorporated into the optimization process as constraints, ensuring that these critical parameters meet predefined thresholds. This approach maintains the structural performance while accommodating the complexity of multi-objective optimization. By combining these advancements, the proposed framework addresses key challenges in structural design, providing a scientifically rigorous methodology for enhancing structural safety, performance, and resilience. The results of this study are expected to contribute significantly to developing advanced optimization strategies and practical applications in engineering.

Proposed by [3], differential evolution (DE) is currently one of the most popular evolutionary algorithms for solving optimization problems in different domains. Three DE-based multi-objective evolutionary algorithms (MOEAs) are adopted in this paper to solve the proposed MOSOPs, such as the success-history-based adaptive multi-objective differential evolution (SHAMODE) and its variation using whale optimization (SHAMODE-WO) [4], in addition to the multi-objective meta-heuristic with iterative parameter distribution estimation (MM-IPDE) [5]. Some studies have demonstrated that these MOEAs perform well on MOSOPs [1,6–8].

Since the MOSOPs proposed in this paper present more than three objective functions, normalized parallel coordinates show the non-dominated solutions. At the same time, multi-criteria decision-making (MCDM) [1,2,9,10] is adopted to extract solutions from the Pareto fronts (PFs) according to the DM's preferences. The MOSOPs analyzed in this paper considered the 25-, 56-, 72-, 120-, and 582-bar trusses inspired by the benchmark optimization problems widely discussed in the literature. The sizing design variables (discrete or continuous) are the cross-sectional areas of the bars.

In summary, this work significantly contributes to the field by addressing gaps in the existing literature. The research's contributions and its novelty are highlighted below:

- Seven novel MOSOPs are proposed. They contain four to seven objective functions, such as maximizing the first natural frequency of vibration and the first critical load factor and also maximizing the difference between some natural frequencies of vibration and the difference between some critical load factors. Due to having more than three objective functions, these seven MOSOPs are classified as many-objective structural optimization problems.
- This study aims to fill the gap regarding broader formulations containing multiple objectives simultaneously, in addition to the two usually considered, reaching up to seven objective functions. This certainly avoids the solution of several structural optimization problems with few objectives, providing the decision-maker with a broader and more complete Pareto front that facilitates and improves the choice of the non-dominated solutions of their preference.
- Three DE-based MOEAs (SHAMODE, SHAMODE-WO, and MM-IPDE) are employed to tackle these new MOSOPs. A comparative analysis is conducted to evaluate the performance of these algorithms on the MOSOPs using several indicators.
- Although many-objective structural optimization problems have the potential to provide the DM with a more comprehensive understanding of the problem, allowing them to make more robust and reliable decisions, these problems have received scant attention in the literature, particularly those with more than four objective functions. Therefore, this study is a significant advancement in filling this gap.

The remainder of this paper is organized as follows. Section 2 presents a literature review on structural optimization problems similar to those discussed in this paper. The MOSOPs proposed in this paper are summarized in Section 3. Section 4 briefly describes the DE-based MOEAs adopted in this paper, the performance indicators used to compare the robustness of each MOEA, and the adopted MCDM used to extract preferred solutions from the PFs. The numerical experiments are described in Section 5. The results are provided and analyzed in Section 6. Finally, Section 7 describes conclusions and future work.

2. Literature Review

For a comprehensive overview of relevant research on structural multi- and many-objective problems incorporating objective functions and constraints within the context of this paper, Table 1 was derived and revised from [1]. One can observe that most works in this table formulated the weight and nodal displacements as the only two conflicting

objective functions, besides the fact that many-objective structural optimization problems have scarcely been explored in the literature.

In Table 1, W represents the weight or total mass of the structure according to each work. f_k represents the i -th natural frequency of vibration, u is the maximum nodal displacement, λ^m is the buckling constraint for member m of the structure, and σ is the allowable stress. NCST is the number of different cross-section types. FRF is the frequency response function, FT is the force transmissibility crest parameter concerning f_k , RMC is the ratio between the maximum compressive load and the critical buckling load at each bar, P_E is the Euler buckling critical load, β is a measure of reliability, and P_f is the probability of failure. CMA is the constrained mass average, SDCV is the standard deviation of the constraints' violations, RI is the reliability index, and RC is the reliability constraint. TPE is the total potential energy, LCC means life-cycle costs, GC refers to geometric constraints, while λ_i indicates the i -th load factor concerning the elastic critical load (global stability).

Other related work to multi-objective structural optimization, including new methodologies, algorithms, applications, etc., can be found in Carvalho et al. [6].

Table 1. Literature review, adapted from [1].

References	Domain	Type	Objective Functions	Constraints
[7,11]	2D	Frame	$W, NCST$	σ, λ^m, u
[6]	2D–3D	Truss	$W, NCST$	σ, λ^m, u
[12]	2D	Frame	CMA, SDCV	σ, λ^m, u
[13]	3D	Truss	$M, 1/\sum_{i=1}^3(F_i u_i)$	σ
[14–16]	2D	Truss	W, u	σ
[10,17–29]	2D–3D	Truss	W, u	σ
[30]	2D–3D	Truss	W, LCC W, f_1	σ σ, λ^m, u
[31]	2D	Truss	W, RI $W, f_1 + f_2 + f_3$ $W, 1/\sum_{i=1}^3 FRF(f_k)$ $W, 1/\sum_{i=1}^3 FT(f_k)$	RC λ^m ad hoc
[32,33]	2D–3D	Truss, frame	W, u	σ
[34]	2D–3D	Truss	$W, TPE, RMC, f_1, f_2, f_3$	u, σ, P_E
[35]	2D	Frame	$W, LCCs$	GC, PH
[36]	2D–3D	Truss	W, u, f_1, TPE W, u, f_1 W, u	σ σ, u σ
[4,37]	2D–3D	Truss	W, β	P_f
[2]	2D–3D	Truss	W, f_1 W, λ_1 W, u	σ, λ_1, u σ, f_1, u σ, λ_1, f_1
[1]	2D–3D	Truss	W, f_1, u W, λ_1, u W, f_1, λ_1 W, f_1, u, λ_1	σ, λ_1 σ, f_1 σ, u σ
[38]	2D–3D	Truss	W, f_1	σ, u
This study	3D	Truss	$W, f_1, f_2 - f_1, f_3 - f_2$ $W, \lambda_1, \lambda_2 - \lambda_1, \lambda_3 - \lambda_2$ $W, f_1, f_2 - f_1, f_3 - f_2, f_4 - f_3$ $W, \lambda_1, \lambda_2 - \lambda_1, \lambda_3 - \lambda_2, \lambda_4 - \lambda_3$ $W, \lambda_1, \lambda_2, \lambda_3, \lambda_2 - \lambda_1, \lambda_3 - \lambda_2$ $W, f_1, f_2, f_3, f_2 - f_1, f_3 - f_2$ $W, f_1, f_2, f_3, \lambda_1, \lambda_2, \lambda_3$	σ, u, λ_1 σ, u, f σ, u, λ_1 σ, u, f σ, u, f σ, u, λ_1 σ, u

3. Many-Objective Structural Optimization Problems

The proposition, formulation, and solution of the seven new MOSOPs presented in this paper are justified since a designer may be very interested in optimizing truss structures with outstanding behaviors regarding their dynamic and global stability performance.

The MOSOPs proposed in this paper are divided into seven formulations, in which the first objective function, the same for all of them, is the minimization of the structure’s weight ($W(\mathbf{x})$), given by

$$W(\mathbf{x}) = \sum_{i=1}^N \rho A_i L_i, \tag{1}$$

where ρ is the material’s specific mass, while A_i and L_i are the cross-sectional area and the length of the i -th bar of the structure, respectively. The number of bars of the truss is denoted by N . The design variables are $\mathbf{x} = \{A_1, A_2, \dots, A_N\}$, where A_i are the sizing design variables indicating the cross-sectional areas of the bars (continuous or discrete). The seven formulations of the MOSOPs are defined in Table 2.

Table 2. Description of each MOSOP.

MOSOP	Type	Objective Functions	Constraints
1	min	$W(\mathbf{x}), -f_1(\mathbf{x}), -(f_2(\mathbf{x}) - f_1(\mathbf{x})), -(f_3(\mathbf{x}) - f_2(\mathbf{x}))$	$\sigma_i(\mathbf{x}) \leq \bar{\sigma}, u_j(\mathbf{x}) \leq \bar{u}_j, \lambda_1(\mathbf{x}) \geq 1$
2	min	$W(\mathbf{x}), -\lambda_1(\mathbf{x}), -(\lambda_2(\mathbf{x}) - \lambda_1(\mathbf{x})), -(\lambda_3(\mathbf{x}) - \lambda_2(\mathbf{x}))$	$\sigma_i(\mathbf{x}) \leq \bar{\sigma}, u_j(\mathbf{x}) \leq \bar{u}_j, f_k(\mathbf{x}) \geq \bar{f}_k$
3	min	$W(\mathbf{x}), -f_1(\mathbf{x}), -(f_2(\mathbf{x}) - f_1(\mathbf{x})), -(f_3(\mathbf{x}) - f_2(\mathbf{x})), -(f_4(\mathbf{x}) - f_3(\mathbf{x}))$	$\sigma_i(\mathbf{x}) \leq \bar{\sigma}, u_j(\mathbf{x}) \leq \bar{u}_j, \lambda_1(\mathbf{x}) \geq 1$
4	min	$W(\mathbf{x}), -\lambda_1(\mathbf{x}), -(\lambda_2(\mathbf{x}) - \lambda_1(\mathbf{x})), -(\lambda_3(\mathbf{x}) - \lambda_2(\mathbf{x})), -(\lambda_4(\mathbf{x}) - \lambda_3(\mathbf{x}))$	$\sigma_i(\mathbf{x}) \leq \bar{\sigma}, u_j(\mathbf{x}) \leq \bar{u}_j, f_k(\mathbf{x}) \geq \bar{f}_k$
5	min	$W(\mathbf{x}), -\lambda_1(\mathbf{x}), -\lambda_2(\mathbf{x}), -\lambda_3(\mathbf{x}), -(\lambda_2(\mathbf{x}) - \lambda_1(\mathbf{x})), -(\lambda_3(\mathbf{x}) - \lambda_2(\mathbf{x}))$	$\sigma_i(\mathbf{x}) \leq \bar{\sigma}, u_j(\mathbf{x}) \leq \bar{u}_j, f_k(\mathbf{x}) \geq \bar{f}_k$
6	min	$W(\mathbf{x}), -f_1(\mathbf{x}), -f_2(\mathbf{x}), -f_3(\mathbf{x}), -(f_2(\mathbf{x}) - f_1(\mathbf{x})), -(f_3(\mathbf{x}) - f_2(\mathbf{x}))$	$\sigma_i(\mathbf{x}) \leq \bar{\sigma}, u_j(\mathbf{x}) \leq \bar{u}_j, \lambda_1(\mathbf{x}) \geq 1$
7	min	$W(\mathbf{x}), -f_1(\mathbf{x}), -f_2(\mathbf{x}), -f_3(\mathbf{x}), -\lambda_1(\mathbf{x}), -\lambda_2(\mathbf{x}), -\lambda_3(\mathbf{x})$	$\sigma_i(\mathbf{x}) \leq \bar{\sigma}, u_j(\mathbf{x}) \leq \bar{u}_j$

In Table 2, $f_k(\mathbf{x})$ is the k -th natural frequency of vibration, $\lambda_l(\mathbf{x})$ is the l -th load factor related to the structure’s global stability, $u_j(\mathbf{x})$ is the displacement of the truss’s j -th node, and $\sigma_i(\mathbf{x})$ is the axial stress at its i -th bar. $\bar{\sigma}$ are \bar{u}_j are the maximum values allowed for the stresses and nodal displacements, respectively, while \bar{f}_k is the minimum value defined for the i -th natural frequency of vibration. If the natural frequency of vibration or the critical load factor are not set as primary objective functions, they are incorporated into the array of constraints. The search space of the design variables is defined by the lower (\mathbf{x}^L) and upper (\mathbf{x}^U) bounds.

The constraints are normalized in the problem formulations, such as

$$\frac{\sigma_i(\mathbf{x})}{\bar{\sigma}} - 1 \leq 0, \quad 1 \leq i \leq m_\sigma, \tag{2}$$

$$\frac{u_j(\mathbf{x})}{\bar{u}_j} - 1 \leq 0, \quad 1 \leq j \leq m_u, \tag{3}$$

$$1 - \frac{f_k(\mathbf{x})}{\bar{f}_k} \leq 0, \quad 1 \leq k \leq m_f, \tag{4}$$

$$1 - \frac{\lambda_1(\mathbf{x})}{1} \leq 0, \tag{5}$$

where m_u is the number of degrees of freedom of the structure, $m_\sigma = N$ is the total number of bars, and m_f is the total number of constrained natural frequencies of vibration. The first critical load factor must be greater than 1, so the load applied to the truss must be no greater than the elastic critical load estimated for the structure, maintaining its global stability.

The static equilibrium equation for a discrete system of bars is used to find the nodal displacements $\{u\}$, written as

$$[K]\{u\} = \{p\}, \quad (6)$$

where $[K]$ is the stiffness matrix and $\{p\}$ are the load components [39].

The natural frequencies of vibration are obtained by solving the eigenvalues of Equation (7):

$$([K] - \omega_i(\mathbf{x})^2[M])\{\Phi_i(\mathbf{x})\} = 0 \quad (7)$$

where $[M]$ is the mass matrix, $\omega_i(\mathbf{x})$ is the i -th natural angular frequency of vibration, and their respective eigenvectors $\{\Phi_i(\mathbf{x})\}$ represent the structure's vibration modes. The smallest eigenvalue ($\omega_1(\mathbf{x})$) corresponds to the first natural angular frequency of vibration, the second smallest ($\omega_2(\mathbf{x})$) to the second angular frequency, and so on.

The load factors λ concerning the global stability are obtained by calculating the eigenvalues of Equation (8):

$$([K] + \lambda_l(\mathbf{x})[K_G])\{\Delta_l(\mathbf{x})\} = 0 \quad (8)$$

where $[K_G]$ is the geometric matrix of the structure, the eigenvalues $\lambda_l(\mathbf{x})$ are the load factors of the structure, and the eigenvectors $\Delta_l(\mathbf{x})$ are the respective instability modes corresponding to each of the critical load factors. The smallest eigenvalue ($\lambda_1(\mathbf{x})$) corresponds to the first critical load factor, the second smallest ($\lambda_2(\mathbf{x})$) to the second load factor, and so on. The matrices $[K]$, $[M]$, and $[K_G]$ can be assembled after transformation to a global axis.

4. Differential Evolution Algorithms, Performance Indicators, and Multi-Criteria Decision-Making (MCDM)

The DE-based MOEAs used to solve the MOSOPs formulated in this paper are the success-history-based adaptive multi-objective differential evolution (SHAMODE) and its variation using whale optimization (SHAMODE-WO), both proposed by Panagant et al. [4], in addition to the multi-objective meta-heuristic with iterative parameter distribution estimation (MM-IPDE) proposed by Wansasueb et al. [5]. These three MOEAs were adopted in this paper due to their superior performance in MOSOPs, which was recently analyzed by Carvalho et al. [6], providing a comparative study involving 15 MOEAs, such as NSGA-II (Deb et al. [40], 2002), GDE3 (Kukkonen and Lampinen [41], 2005), MOEA/D (Zhang and Li [42], 2007), DEMO (Tušar and Bogdan [43], 2009), UPS-EMOA (Aittokoski and Miettinen [44], 2010), RPBILDE (Pholdee and Bureerat [45], 2013), MOWCA (Sadollah et al. [46], 2015), MODA (Mirjalili [47], 2016), MOGWO (Mirjalili et al. [48], 2017), MOALO (Mirjalili et al. [49], 2017), MSSA (Mirjalili et al. [50], 2017), MOMVO (Mirjalili et al. [51], 2017), and MOGOA (Mirjalili et al. [52], 2018).

SHAMODE is an adaptive differential evolution algorithm for multi-objective optimization problems. It is characterized by adapting the parameters F and P_{cr} of the original DE based on successful results in previous generations of solutions. This adaptation method was initially proposed by Tanabe and Fukunaga [53]. A random population starts SHAMODE, subjected to an evolution process involving mutation, cross-over, and selection. Creating an empty external file (A_0) is initially necessary. At the end of each generation, the index i of individuals that survived the evolutionary process is stored in the vector $_{sind}$. From these indices, the vectors $\mathbf{x}_{sind,g}$, which generated successful descendants, are sent to the external file A_{g+1} . If $_{sind}$ is not an empty vector, the mean values of the parameters F and P_{cr} of its individuals are calculated. These mean values are stored in the memory vectors M_F and $M_{P_{cr}}$. SHAMODE-WO is a variation of SHAMODE, which differs from its

predecessor in the mutation process, in which the Spiral Movement Operator (extracted from the whale optimization algorithm [54]) is added.

The last algorithm used was the MM-IPDE. This meta-heuristic also adapts the DE parameters. However, while SHAMODE and SHAMODE-WO adapt the parameters F and P_{cr} based on the success of previous individuals, MM-IPDE performs this process through an optimization algorithm that acts in binary search spaces, called population-based incremental learning for multi-objective optimization (PBILM), developed in [55]. In addition to the parameter adaptation, PBILM is also used to choose the mutation and crossover processes to be applied in the evolutionary process of the multi-objective optimization problems. This algorithm is based on population-based incremental learning (PBIL), proposed in [56] for single-objective problems.

Studies in the literature show that these MOEAs are effective for MOSOPs [1,6–8]. For instance, Carvalho et al. [6] showed that MM-IPDE outperformed 15 other MOEAs. Constraint handling utilized either the constraint-based non-dominated sorting technique [40] or constraint dominance principles. Under these principles, the following points occur: (i) feasible solutions are prioritized over infeasible ones; (ii) among infeasible solutions, those with smaller constraint violations are ranked higher; and (iii) among feasible solutions, dominance determines the ranking. In the computational experiments conducted here, the algorithms were configured according to the parameters specified in their original references.

One of the objectives of this study is to compare the performances of the meta-heuristics used to solve the formulated MOSOPs. For this purpose, well-known performance indicators from the literature are applied, such as the hypervolume (HV) [57] and the IGD+ [58], from which the performance profiles (PPs) [59] of the algorithms are drawn. PPs were introduced by Dolan and Moré [59], and they can compare the performance of several algorithms concerning a total set of the numerical results of a set of numerical experiments. According to Barbosa et al. [60], the area under the curve of the PPs generated by a given algorithm is an indicator of the general performance of the algorithm in solving a subset of the whole set of problems. This metric is also used to compare the meta-heuristics applied in this work. The larger the obtained area, the better the efficiency of the analyzed algorithm.

Once the Pareto fronts are obtained, the DM faces the task of selecting the solutions of interest. In this study, the multi-criteria tournament decision (MTD) method proposed by Parreiras and Vasconcelos [9] is employed to extract the desired solutions from the Pareto fronts obtained in each MOSOP. Derived from the MCDM framework, this method ranks the best and worst solutions based on the objective function values and the weights (w_i) assigned to them by the decision-maker. The proposed methodology of this study is illustrated in the flowchart provided in Figure 1.

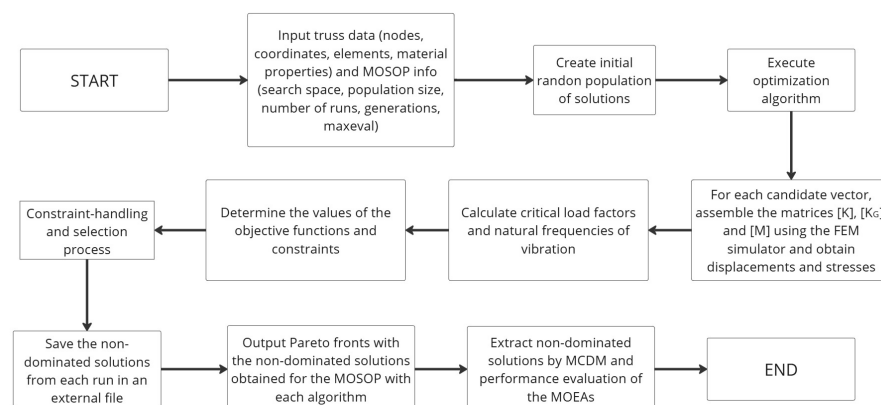


Figure 1. Flowchart of the proposed methodology.

5. Computational Experiments

This section presents the spatial trusses to be optimized in this paper. The 25-, 56-, 72-, 120-, and 582-bar trusses are depicted in Figures 2–6 and are subjected to the seven MOSOPs described in Section 3, solved through the three DE-based algorithms described in Section 4. In the results, these trusses are denoted by T25, T56, T72, T120, and T582. Characteristics and descriptions of the trusses, such as loading cases, materials, search spaces, the grouping of the bars, etc., are detailed and can be found, for instance, in [1,61]. The population sizes were 20 and 30 for the 25- and 56-bar trusses, respectively, and 50 for the 72-, 120-, and 582-bar trusses. The number of generations was 100 for the 25- and 56-bar trusses and 200 for the 72-, 120-, and 582-bar trusses. The maximum number of function evaluations was 2000 for the 25-bar truss and 3000 for the 56-bar truss, whereas for the 72-, 120-, and 582-bar trusses, it was 10000. The independent runs were 30 and 10 for the 25- and 56-bar trusses, respectively, and 20 for the 72-, 120-, and 582-bar trusses.

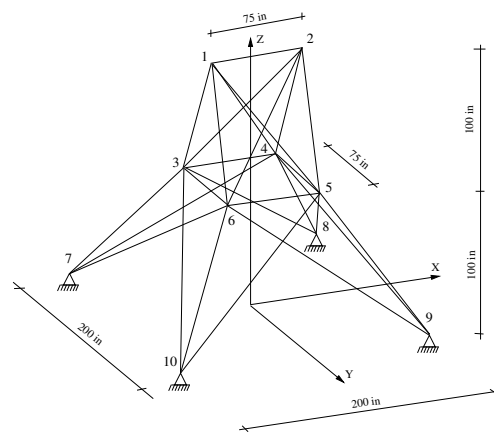


Figure 2. 25-bar truss.

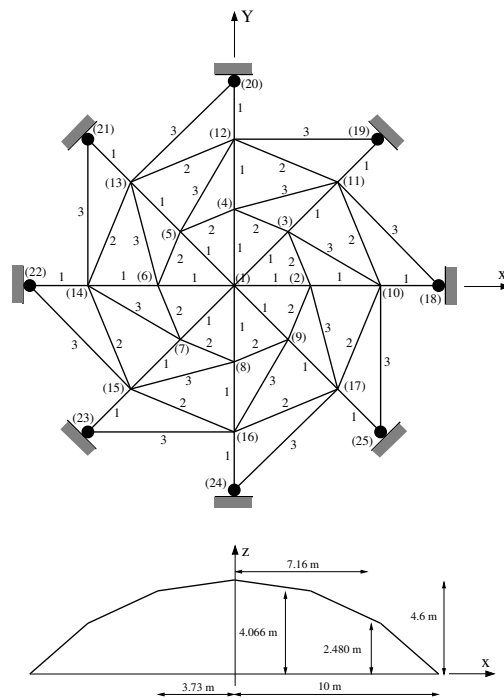


Figure 3. 56-bar truss.

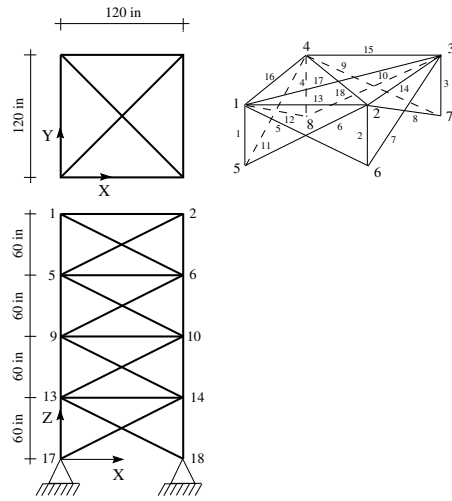


Figure 4. 72-bar truss.

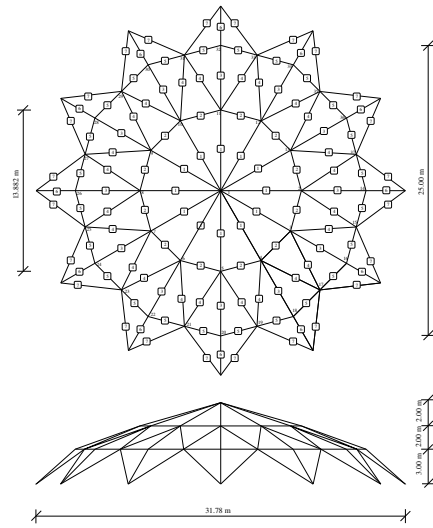


Figure 5. 120-bar truss.

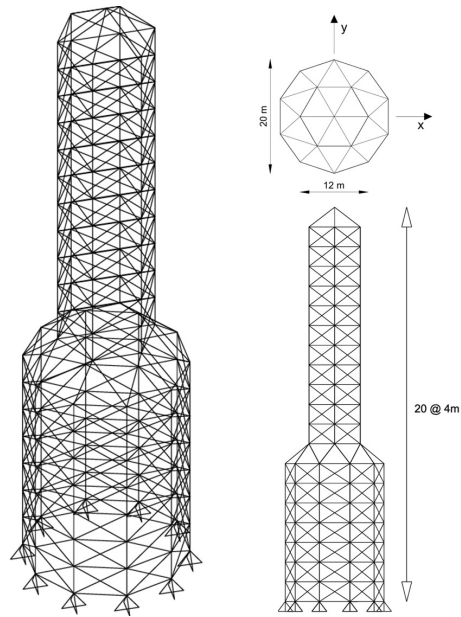


Figure 6. 582-bar truss.

6. Results

This section presents the results obtained with the solution of the MOSOPs in the proposed trusses through the three DE-based algorithms. PFs using parallel coordinates provide the non-dominated solutions obtained for the problems by each algorithm. The desired solutions are extracted from these PFs through the MTD method according to the DM's preferences. Finally, the HV and IGD+ performance indicators compare the algorithm's performance.

6.1. Parallel Coordinates and Extracted Solutions

As mentioned in Section 5, each truss in this study is subjected to the seven MOSOPs presented in Section 3 and solved through the three DE-based algorithms described in Section 4. The MTD method extracts the desired solution from the PFs for each problem according to the DM's preferences, setting weights w_i of importance, in which the sum of w_i must be equal to 1 (see [9] for details on these weights). For this purpose, the DM must indicate the weight/importance of each objective function in this selection process. In this paper, two comparison scenarios are used: sc_1 with equal weights for all objective functions (four objectives: $w_1 = 1/4$, $w_2 = 1/4$, $w_3 = 1/4$, and $w_4 = 1/4$; five objectives: $w_1 = 1/5$, $w_2 = 1/5$, $w_3 = 1/5$, $w_4 = 1/5$, and $w_5 = 1/5$; seven objectives: $w_1 = 1/7$, $w_2 = 1/7$, $w_3 = 1/7$, $w_4 = 1/7$, $w_5 = 1/7$, $w_6 = 1/7$, and $w_7 = 1/7$) and sc_2 with a weight of 0.5 for the minimization of $W(\mathbf{x})$ and equal weights amongst themselves to the other objective functions (four objectives: $w_1 = 0.5$, $w_2 = 0.5/3$, $w_3 = 0.5/3$, and $w_4 = 0.5/3$; five objectives: $w_1 = 0.5$, $w_2 = 0.5/4$, $w_3 = 0.5/4$, $w_4 = 0.5/4$, and $w_5 = 0.5/4$; seven objectives: $w_1 = 0.5$, $w_2 = 0.5/6$, $w_3 = 0.5/6$, $w_4 = 0.5/6$, $w_5 = 0.5/6$, $w_6 = 0.5/6$, and $w_7 = 0.5/6$), favoring the extraction of lighter structural solutions.

Each solution's objective function values are normalized to generate the parallel coordinates. Knowing that of_{max} , of_{min} and $of(\mathbf{x})$ are, respectively, the maximum value obtained, the minimum value, and the value of the objective function of in the solution \mathbf{x} , this normalization is calculated by

$$\frac{of(\mathbf{x}) - of_{min}}{of_{max} - of_{min}}. \quad (9)$$

The y -axis varies from 0 to 1, from the minimum to the maximum value obtained for each objective function among all non-dominated solutions. The x -axis has values from 1 to N_F (number of objectives in the problem) to indicate the normalized values obtained for each function. Each line drawn is one non-dominated solution obtained, following the color pattern: red for MM-IPDE solutions, blue for SHAMODE, and yellow for SHAMODE-WO. The parallel coordinate PFs for the MOSOPs are presented in the traditional flat form and from a three-dimensional point of view, highlighting the solutions provided by each applied algorithm.

To illustrate the results concerning the PFs of the seven MOSOPs, MOSOPs 1, 4, and 7 are selected and exhibited.

6.2. Pareto Fronts for MOSOP1

The MTD solutions obtained in the sc_1 scenario are highlighted in green, and the solutions extracted with the sc_2 weights are highlighted in cyan in the respective PFs presented in the next subsection.

From the PF obtained for the 25-bar truss in Figure 7a,b (MOSOP1), where each line represents a non-dominated solution, it is possible to observe that these lines intersect between the four objectives, indicating a conflict between them. For example, the weight $W(\mathbf{x})$ is the first objective function (minimized), and the natural frequency of vibration

$f_1(\mathbf{x})$ is the second objective function (maximized). The same happens between the weight and the other objective functions, such as $(f_2(\mathbf{x}) - f_1(\mathbf{x}), (f_3(\mathbf{x}) - f_2(\mathbf{x}))$. Regarding the extracted solutions, according to the sc_1 and sc_2 scenarios, it can be observed that for sc_2 , where 50% is prioritized for the weight, the MTD indicated, as expected, a non-dominated solution with a weight of the order of 20% (0.2 on the vertical axis of Figure 7a) of the heaviest non-dominated solution. On the other hand, the second objective function is in the order of 75% of the non-dominated solution with the highest natural frequency of vibration. The other objective functions of the extracted solutions presented values close to 20% and 40% for the two scenarios. The complete details of the extracted solutions, such as the values of the design variables, objective functions, and constraints, are shown in tables presented further in this text. From Figure 7b, it is important to observe that the PFs obtained by the three MOEAs present a similar distribution of non-dominated solutions.

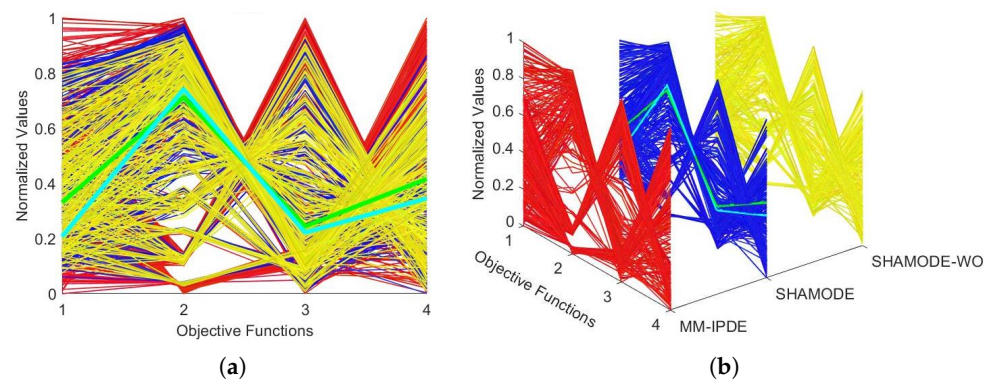


Figure 7. Normalized parallel coordinates PF for the 25-bar truss dome for MOSOP1. (a) Two dimensions. (b) Three dimensions.

Figure 8a,b present the PFs for the 56-bar truss. As in the PFs obtained for the 25-bar truss, a crossing of the lines corresponding to each non-dominated solution is observed, indicating the conflict between the objective functions. It is noted that the extracted solutions, according to the preferences of the artificial DM, coincidentally indicated the same solutions for both sc_1 and sc_2 . However, several other non-dominated solutions could be extracted by the artificial DM. Furthermore, for sc_1 , where the weight is prioritized at 50% compared to the other objective functions, the solution found obtained 0.2 of the normalized value corresponding to the non-dominated solution with the highest weight. From Figure 8b, it is important to observe that the PFs obtained by the three MOEAs present a similar distribution of non-dominated solutions.

Figure 9a,b present the PFs for the 72-bar truss. The intersection of the lines representing the non-dominated solutions can be observed, indicating that the objective functions are conflicting. The extracted solutions were approximately 30%, 40%, 10%, and 40%, respectively, of the maximum values for sc_1 and 41%, 68%, 20%, and 50%, respectively, of the maximum values for sc_2 . From Figure 9b, it is important to note that the PFs obtained by the three MOEAs present a similar distribution of non-dominated solutions.

Figure 10a,b present the PFs for the 120-bar truss. The extracted non-dominated solutions were approximately 40%, 78%, 80%, and 0%, respectively, of the maximum values for sc_1 and 20%, 63%, 70%, and 0%, respectively, of the maximum values for sc_2 . For the fourth objective function, the artificial DM indicated non-dominated solutions with the lowest values among all the PFs. From Figure 10b, it is important to observe that the PFs obtained by the three MOEAs present a similar distribution of non-dominated solutions.

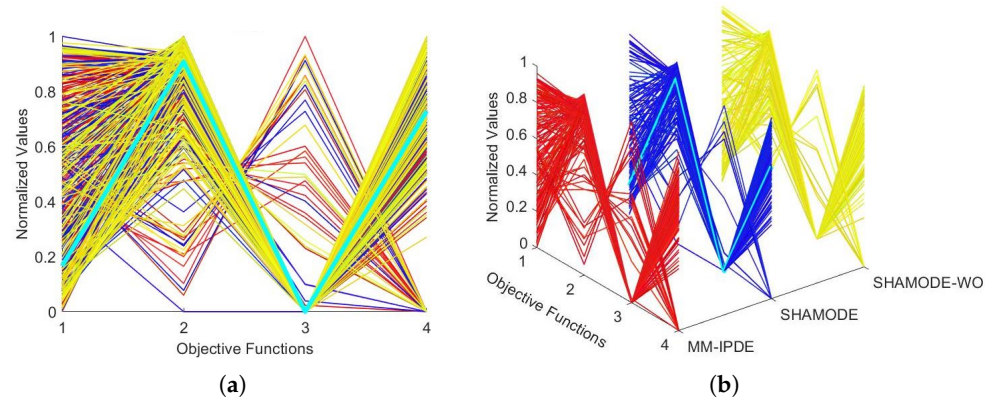


Figure 8. Normalized parallel coordinates PF for the 56-bar truss dome for MOSOP1. (a) Two dimensions. (b) Three dimensions.

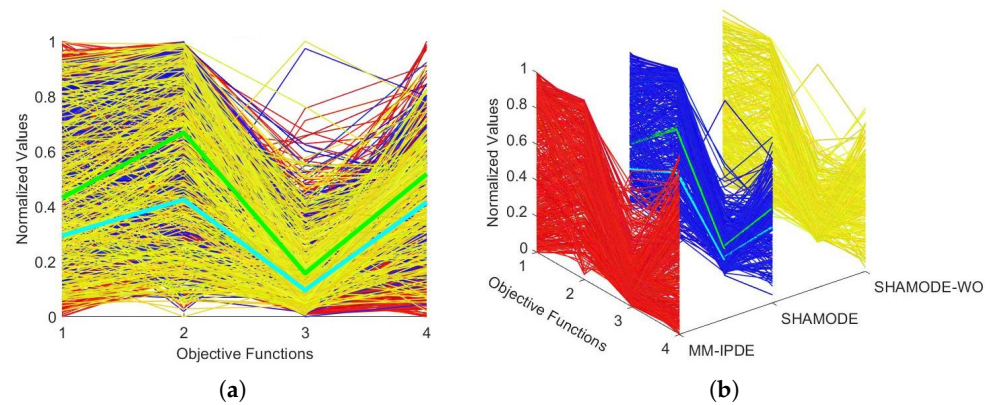


Figure 9. Normalized parallel coordinates PF for the 72-bar truss dome for MOSOP1. (a) Two dimensions. (b) Three dimensions.

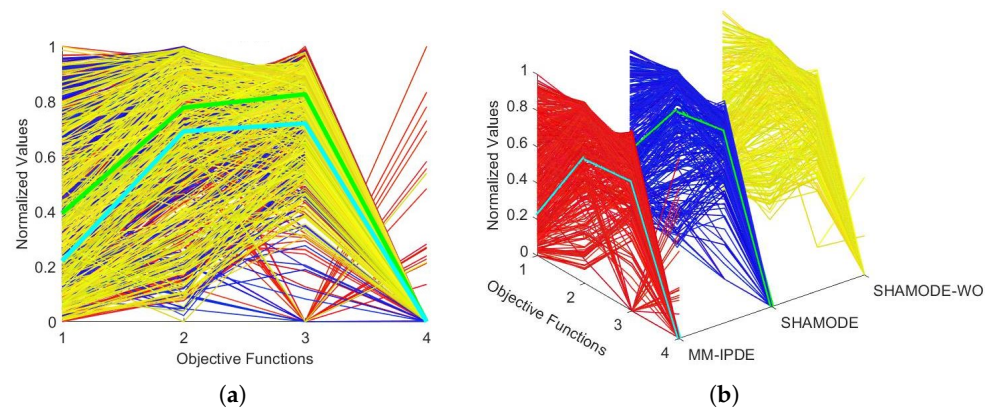


Figure 10. Normalized parallel coordinates PF for the 120-bar truss dome for MOSOP1. (a) Two dimensions. (b) Three dimensions.

Figure 11a,b present the PFs for the last MOSOP1, referring to the 582-bar truss, where a very evident behavior regarding the conflict of the objective functions is again observed, as occurred in the 25-bar and 56-bar trusses. The extracted solutions were approximately 30%, 42%, 50%, and 62%, respectively, of the maximum values for sc_1 and 18%, 40%, 38%, and 58%, respectively, of the maximum values for sc_2 . From Figure 11b, it is important to observe that the PFs obtained by the three MOEAs present a similar distribution of non-dominated solutions.

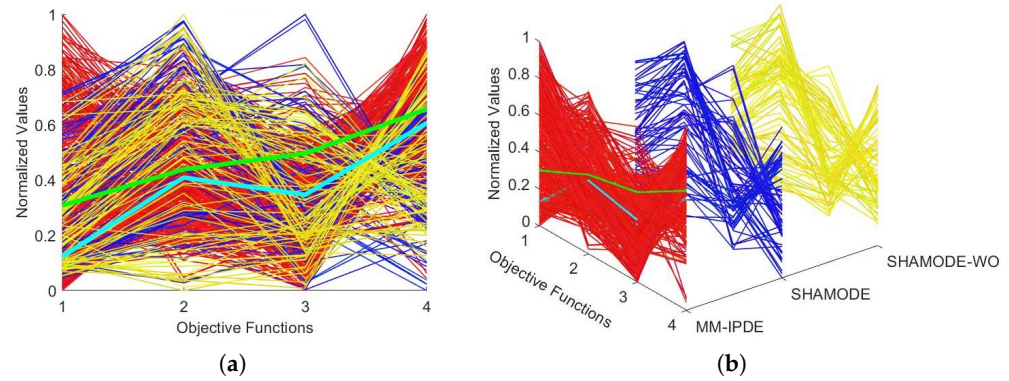


Figure 11. Normalized parallel coordinates PF for the 582-bar truss dome for MOSOP1. (a) Two dimensions. (b) Three dimensions.

6.3. Pareto Fronts for MOSOP4

Figure 12a,b present the PFs for the 25-bar truss. Figure 12a shows that the PFs obtained by the three MOEAs present a similar distribution of non-dominated solutions. In this experiment, despite being conflicting, there is no significant crossover between objectives one and two. However, this occurs among the other objectives, for example, between objectives two, three, four, and five. The extracted solutions were approximately 57%, 62%, 40%, 22%, and 63%, respectively, of the maximum values for sc_1 and 35%, 56%, 38%, 22%, and 60%, respectively, of the maximum values for sc_2 .

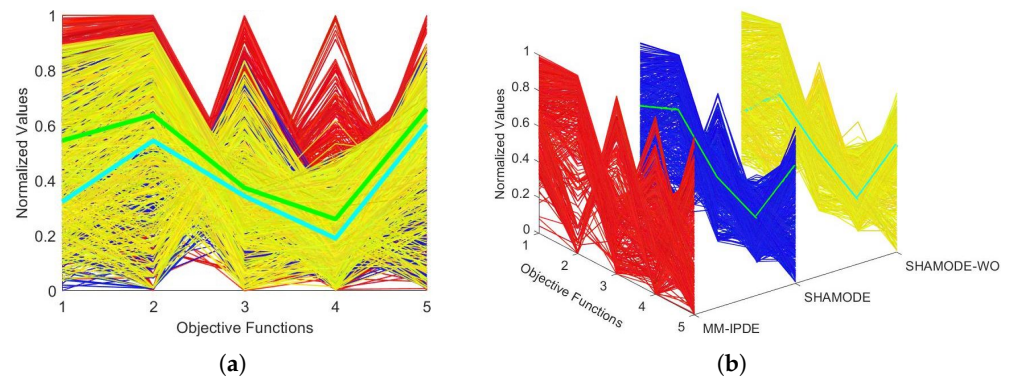


Figure 12. Normalized parallel coordinates PF for the 25-bar truss dome for MOSOP4. (a) Two dimensions. (b) Three dimensions.

Figure 13a,b present the PFs for the 56-bar truss. In the case of this computational experiment, in addition to a very similar behavior among the solutions obtained by the three MOEAs, a good distribution of solutions along the lower and upper limits for the objective functions was also observed. The extracted solutions were approximately 58%, 56%, 42%, 70%, and 22%, respectively, of the maximum values for sc_1 and 30%, 35%, 28%, 39%, and 18%, respectively, of the maximum values for sc_2 .

Figure 14a,b present the PFs for the 72-bar truss. From the PFs shown in Figure 14a,b, it can be observed that there is a good distribution of solutions not dominated by the three MOEAs for all objective functions except for the third one, which concentrated most of the solutions in the lowest normalized values (i.e., close to zero). The extracted solutions were approximately 42%, 75%, 0%, 40%, and 20%, respectively, of the maximum values for sc_1 and 30%, 58%, 0%, 24%, and 20%, respectively, of the maximum values for sc_2 . Again, the three MOEAs achieved very similar PFs.

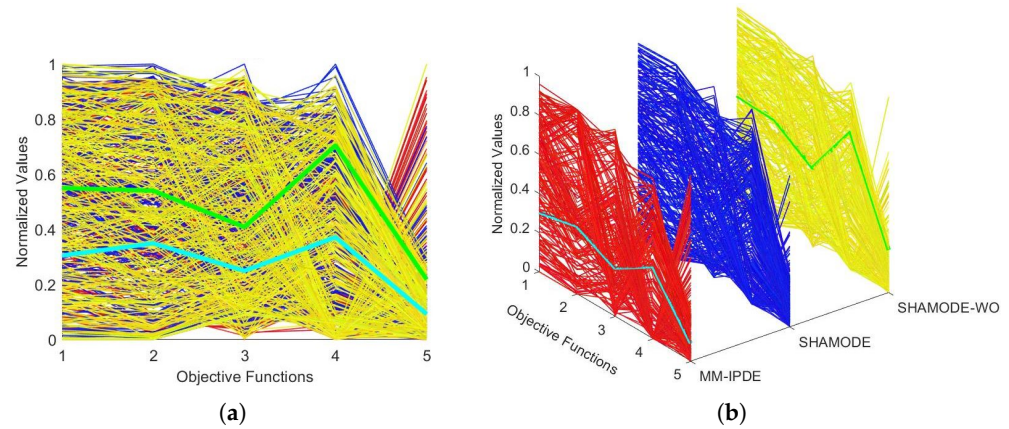


Figure 13. Normalized parallel coordinates PF for the 56-bar truss dome for MOSOP4. (a) Two dimensions. (b) Three dimensions.

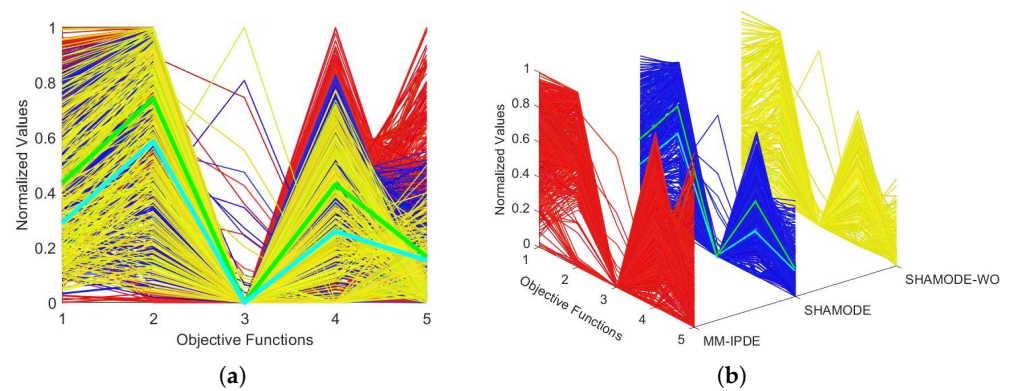


Figure 14. Normalized parallel coordinates PF for the 72-bar truss dome for MOSOP4. (a) Two dimensions. (b) Three dimensions.

Figure 15a,b present the PFs for the 120-bar truss. There is a good distribution of non-dominated solutions between the maximum and minimum values of each objective function in addition to the similar PFs obtained by each MOEA. The extracted solutions were approximately 40%, 95%, 90%, 22%, and 85%, respectively, of the maximum values for sc_1 and 28%, 60%, 55%, 15%, and 50%, respectively, of the maximum values for sc_2 . Again, the three MOEAs achieved very similar PFs.

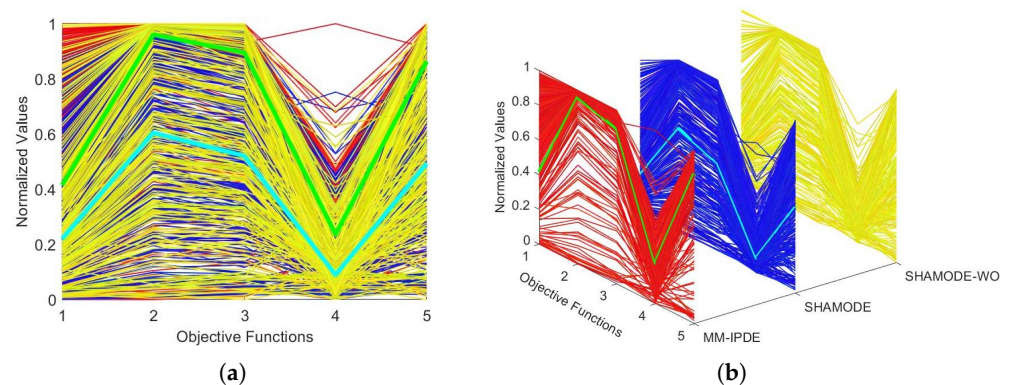


Figure 15. Normalized parallel coordinates PF for the 120-bar truss dome for MOSOP4. (a) Two dimensions. (b) Three dimensions.

Figure 16a,b present the PFs for the 582-bar truss. Observing the PFs obtained for this experiment, it is noted that the MOEAs did not present much similarity except between those obtained by the SHAMODE and SHAMODE-WO algorithms. However, this is a

very interesting characteristic because the PFs complement each other, providing a more comprehensive distribution of non-dominated solutions. The extracted solutions were approximately 24%, 38%, 22%, 16%, and 18%, respectively, of the maximum values for sc_1 and 17%, 18%, 19%, 13%, and 16%, respectively, of the maximum values for sc_2 .

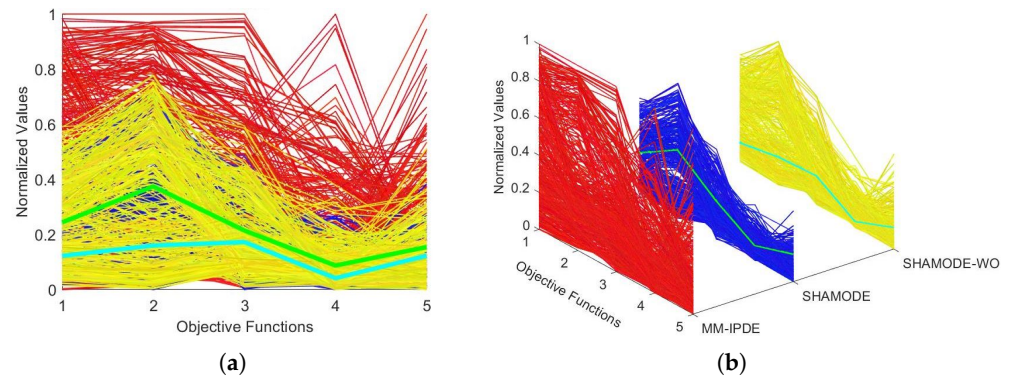


Figure 16. Normalized parallel coordinates PF for the 582-bar truss dome for MOSOP4. (a) Two dimensions. (b) Three dimensions.

6.4. Pareto Fronts for MOSOP7

Figure 17a,b present the PFs for the 25-bar truss. For this experiment, again, the PFs obtained by each MOEA are quite similar, and there is also a good distribution of solutions between the maximum and minimum values of each objective function. The extracted solutions were approximately 50%, 90%, 22%, 82%, 78%, 72%, 71%, and 40%, respectively, of the maximum values for sc_1 and 22%, 88%, 79%, 42%, 41%, 50%, and 20%, respectively, of the maximum values for sc_2 .

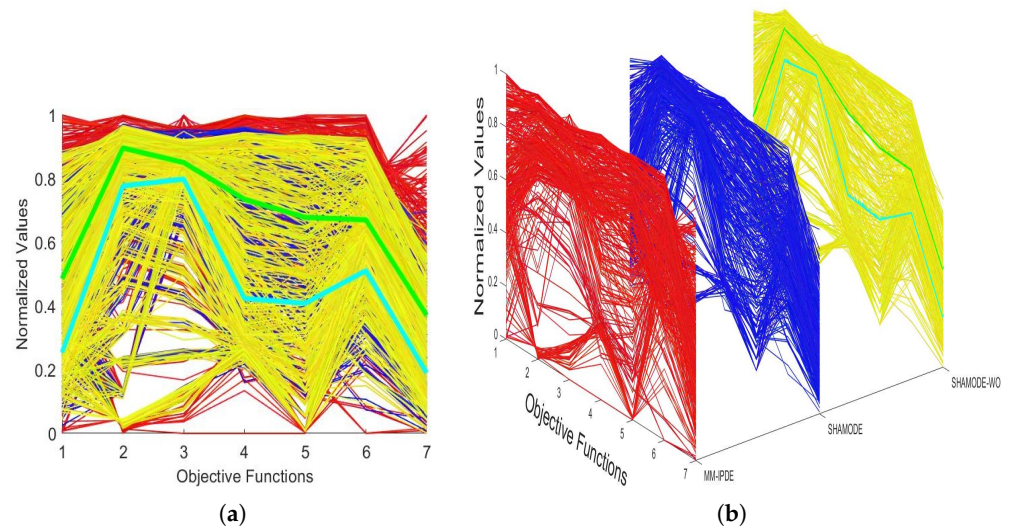


Figure 17. Normalized parallel coordinates PF for the 25-bar truss dome for MOSOP7. (a) Two dimensions. (b) Three dimensions.

Figure 18a,b present the PFs for the 56-bar truss. It is noted that the PFs obtained by the three MOEAs for this experiment comprise one of the most distributed solutions between the maximum and minimum values of the seven objective functions among the experiments analyzed in this paper. This indicates that the DM can choose many solutions according to their preferences. The extracted solutions were approximately 43%, 78%, 78%, 85%, 48%, 45%, and 46%, respectively, of the maximum values for sc_1 and 21%, 50%, 50%, 100%, 20%, 20%, and 21%, respectively, of the maximum values for sc_2 .

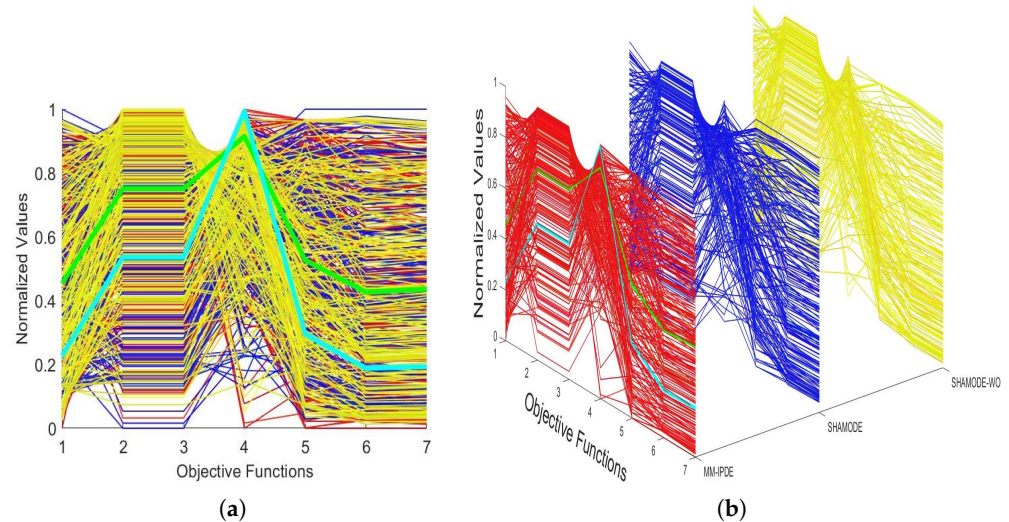


Figure 18. Normalized parallel coordinates PF for the 56-bar truss dome for MOSOP7. (a) Two dimensions. (b) Three dimensions.

Figure 19a,b present the PFs for the 72-bar truss. One can observe, again, that the PFs obtained by the three MOEAs for this experiment comprise, as in the case of the 56-bar truss, one of those that most distributed solutions along the maximum and minimum values among the seven objective functions. Again, as in the previous case, this is a good indication for the DM of the possibility of choosing numerous solutions according to their preferences. The extracted solutions were approximately 42%, 68%, 68%, 74%, 52%, 52%, and 50%, respectively, of the maximum values for sc_1 and 21%, 42%, 43%, 43%, 30%, 30%, and 33%, respectively, of the maximum values for sc_2 .

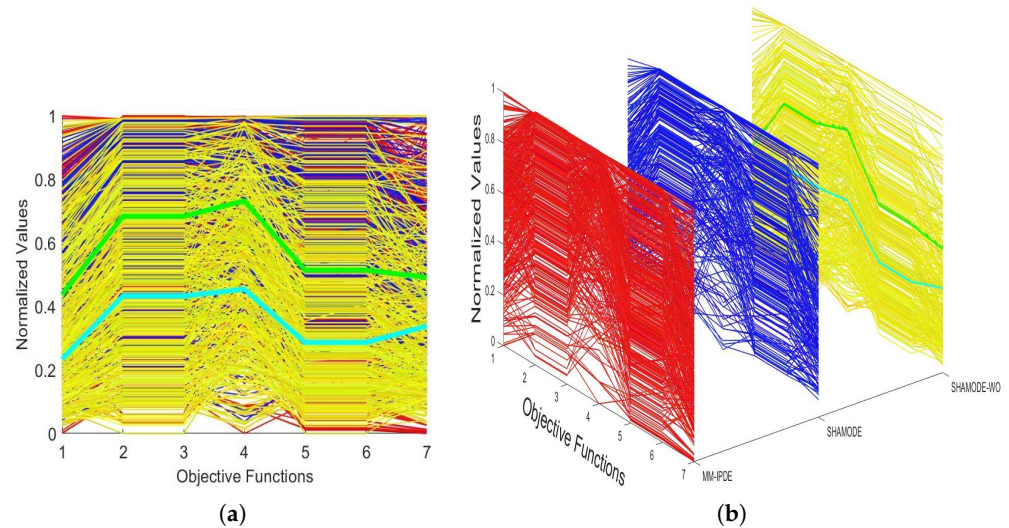


Figure 19. Normalized parallel coordinates PF for the 72-bar truss dome for MOSOP7. (a) Two dimensions. (b) Three dimensions.

Figure 20a,b present the PFs for the 120-bar truss. The PFs obtained by the three MOEAs in this experiment, similar to those for the 56-bar and 72-bar trusses, demonstrate evenly distributed sets of solutions across the maximum and minimum values of the seven objective functions. As in the previous cases, this gives the DM a strong indication of the availability of numerous solutions based on their preferences. The extracted solutions were approximately 21%, 97%, 95%, 96%, 98%, 98%, and 98%, respectively, of the maximum

values for sc_1 and 50%, 83%, 82%, 82%, 57%, 56%, and 56%, respectively, of the maximum values for sc_2 .

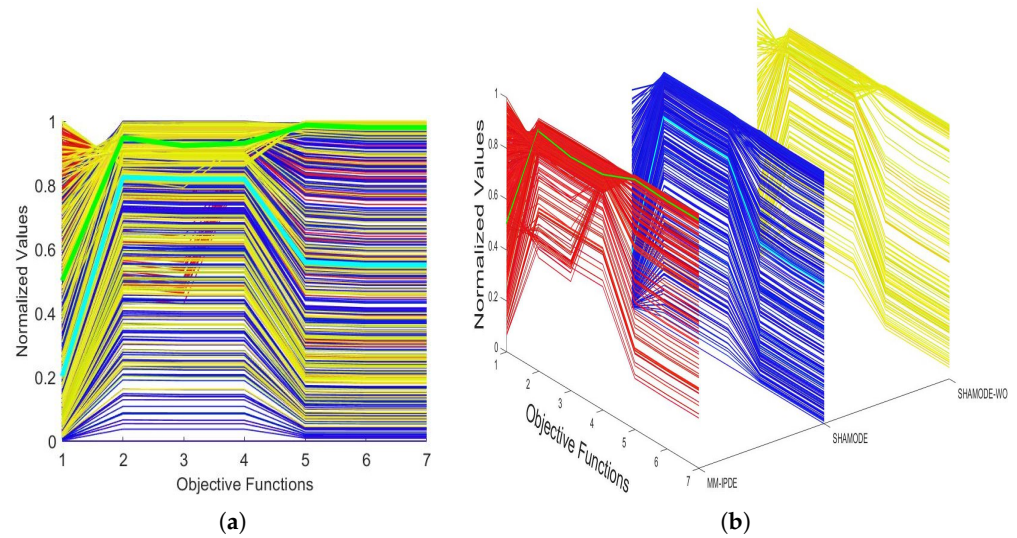


Figure 20. Normalized parallel coordinates PF for the 120-bar truss dome for MOSOP7. (a) Two dimensions. (b) Three dimensions.

Figure 21a,b present the PFs for the 582-bar truss. This experiment shows a good distribution of non-dominated solutions between the maximum and minimum values of the normalized objective functions, except for the fourth and seventh objective functions. The extracted solutions were approximately 28%, 57%, 58%, 62%, 34%, 36%, and 22%, respectively, of the maximum values for sc_1 and 17%, 28%, 28%, 64%, 20%, 19%, and 18%, respectively, of the maximum values for sc_2 .

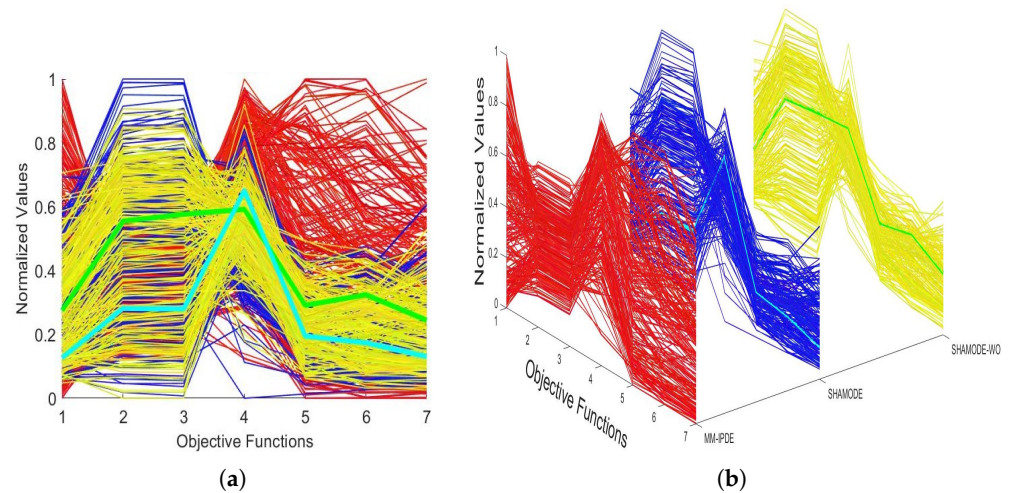


Figure 21. Normalized parallel coordinates PF for the 582-bar truss dome for MOSOP7. (a) Two dimensions. (b) Three dimensions.

6.5. Complete Data of the Non-Dominated Extracted Solutions

Table 3 provides detailed information on the extracted non-dominated solutions for scenarios sc_1 and sc_2 of MOSOP1. This table presents the design variables (cross-sectional areas of the bars), the DE-based algorithm that provided the extracted solution, and the values of the objective functions. For the 25-bar truss, the final weight of the truss considering sc_2 (i.e., the weight has a 50% preference over the other objectives) was 276.97 kg vs. 310.62 kg for sc_1 , where the preferences are equal among all objectives. The sc_2 solution is 10.83% lighter.

As stated earlier in this text, the solutions extracted by the artificial DM were the same for both scenarios for the 56-bar truss, presenting the final weight equal to 1039.89 kg. The weight of the solution extracted for the 72-bar truss was 754.86 kg considering sc_1 and 576.96 for sc_2 , resulting in approximately a 31.14% difference between the largest and smallest weights. For the 120-bar truss, the weights of the extracted solutions were 29,054.60 kg and 19,863.97 kg for sc_1 and sc_2 , respectively, resulting in a difference of 46.27%. Finally, 804,249.40 kg and 441,471.98 kg were the weights of the solutions extracted from the 582-bar truss, leading to a difference of 82.17%. These results show how multi-objective optimization can generate a set of solutions with significant differences in the optimal design's final weight, which may interest the DM according to their preferences.

Table 3. Values obtained for the design variables and objective functions of the MTD solutions extracted from MOSOP1.

A_i (cm ²)	T25		T56		T72		T120		T582	
Scenario	sc_1	sc_2	sc_1	sc_2	sc_1	sc_2	sc_1	sc_2	sc_1	sc_2
D. Var.	SHAMODE	MM-IPDE	MM-IPDE	MM-IPDE						
1	2.5806	1.2903	5.2029	5.2029	3.2346	11.4148	77.3516	62.9779	145.8062	276.7736
2	5.1613	5.8064	4.9074	4.9074	19.2092	9.8772	32.1194	27.9390	806.4500	398.7089
3	15.4838	16.1290	5.1576	5.1576	7.6113	5.3282	16.3207	18.4665	156.7739	178.7093
4	11.6129	1.2903	-	-	0.9813	3.1062	85.5466	61.6680	1148.3848	193.5480
5	6.4516	2.5806	-	-	6.8117	23.5284	73.3268	59.8157	212.2576	136.1288
6	12.9032	8.3871	-	-	21.1769	12.4921	34.8597	39.4141	366.4509	87.0966
7	19.3548	18.0645	-	-	0.8122	1.8269	49.7527	7.2751	181.9351	193.5480
8	16.1290	18.0645	-	-	5.7710	1.1051	-	-	76.1289	275.4833
9	-	-	-	-	22.9382	13.6429	-	-	94.1934	39.7419
10	-	-	-	-	19.4474	15.5892	-	-	337.4187	210.9673
11	-	-	-	-	6.7520	8.8941	-	-	64.5160	366.4509
12	-	-	-	-	1.1405	3.3575	-	-	864.5144	189.6770
13	-	-	-	-	16.5387	8.1441	-	-	487.7410	159.9997
14	-	-	-	-	20.4564	13.7697	-	-	81.2902	101.9353
15	-	-	-	-	1.2561	8.6291	-	-	1148.3848	305.8058
16	-	-	-	-	4.2488	1.7057	-	-	651.6116	145.8062
17	-	-	-	-	-	-	-	-	1264.5136	227.7415
18	-	-	-	-	-	-	-	-	276.7736	68.3870
19	-	-	-	-	-	-	-	-	39.7419	39.7419
20	-	-	-	-	-	-	-	-	651.6116	248.3866
21	-	-	-	-	-	-	-	-	301.2897	39.7419
22	-	-	-	-	-	-	-	-	39.7419	39.7419
23	-	-	-	-	-	-	-	-	948.3852	276.7736
24	-	-	-	-	-	-	-	-	76.1289	39.7419
25	-	-	-	-	-	-	-	-	94.8385	39.7419
26	-	-	-	-	-	-	-	-	478.0636	178.7093
27	-	-	-	-	-	-	-	-	66.4515	72.2579
28	-	-	-	-	-	-	-	-	39.7419	167.0964
29	-	-	-	-	-	-	-	-	176.1287	113.5482
30	-	-	-	-	-	-	-	-	216.1286	39.7419
31	-	-	-	-	-	-	-	-	56.7096	127.0965
32	-	-	-	-	-	-	-	-	149.6771	39.7419
W (kg)	310.62	276.97	1039.89	1039.89	754.86	576.96	29,054.60	19,863.97	804,249.40	441,471.98
f_1 (Hz)	37.42	38.35	26.20	26.20	3.79	3.11	5.52	5.17	1.56	1.51
$f_2 - f_1$ (Hz)	7.77	7.05	0	0	0	0	0.12	0.10	0.09	0.07
$f_3 - f_2$ (Hz)	10.77	8.95	10.31	10.31	2.80	2.34	0	0	2.60	2.44

Table 4 provides detailed information on the extracted non-dominated solutions for scenarios sc_1 and sc_2 of MOSOP4. For the 25-bar truss, the weights of the non-dominated extracted solutions were 373.86 kg and 313.35 kg, respectively, for the sc_1 and sc_2 scenarios, resulting in a difference of approximately 19.31% in favor of the heavier structure. A difference of 59.55% was found between the final weights of the solutions extracted by the sc_1 and sc_2 scenarios of the 56-bar truss, i.e., 2507.94 kg and 1571.82 kg. For the 72-bar truss, the difference was 15.63% between the weights of the two extracted solutions, i.e., 988.60 kg vs. 854.96 kg. For the 120-bar truss, the weights of the extracted solutions were 35,124.35 vs. 23,863.82 kg, resulting in a difference of approximately 47.18% more for the heavier structure. For the 582-bar truss, the difference was 65.79% for the weights of 967,602.87 kg vs. 583,624.36 kg.

Table 4. Values obtained for the design variables and objective functions of the MTD solutions extracted from MOSOP4.

A_i (cm ²)	T25		T56		T72		T120		T582	
Scenario	sc_1	sc_2	sc_1	sc_2	sc_1	sc_2	sc_1	sc_2	sc_1	sc_2
D. Var.	SHAMODE	SHAMODE-WO	SHAMODE-WO	MM-IPDE	SHAMODE	SHAMODE	MM-IPDE	SHAMODE	SHAMODE	SHAMODE-WO
1	18.0645	5.1613	8.8874	7.7869	18.0534	22.1119	83.9015	51.7107	227.7415	359.9993
2	16.7742	9.6774	16.3196	9.3201	17.5776	8.6566	33.6933	44.5132	1045.1592	181.9351
3	18.0645	18.0645	12.7513	6.6403	20.9335	9.8552	18.5951	14.1340	226.4512	129.0320
4	10.9677	19.3548	-	-	2.5878	3.2963	140.0000	85.6471	193.5480	183.8706
5	16.7742	15.4838	-	-	12.6018	16.7091	70.7834	38.3752	212.2576	183.8706
6	16.7742	13.5484	-	-	16.9417	15.6065	35.9559	28.0943	1387.0940	129.0320
7	12.9032	12.2580	-	-	9.2325	15.4614	15.5746	11.7173	231.6124	589.6762
8	20.6451	16.1290	-	-	3.5346	1.7020	-	-	278.7091	189.6770
9	-	-	-	-	25.6897	24.3596	-	-	399.9992	66.4515
10	-	-	-	-	25.3886	21.8002	-	-	76.1289	110.3224
11	-	-	-	-	22.8431	15.5750	-	-	193.5480	129.0320
12	-	-	-	-	12.4678	2.2205	-	-	948.3852	589.6762
13	-	-	-	-	25.6171	25.3965	-	-	399.9992	250.3221
14	-	-	-	-	19.7497	24.9362	-	-	197.4190	178.7093
15	-	-	-	-	10.7487	1.3154	-	-	864.5144	257.4188
16	-	-	-	-	6.1029	13.2372	-	-	216.1286	107.7417
17	-	-	-	-	-	-	-	-	1045.1592	250.3221
18	-	-	-	-	-	-	-	-	178.7093	398.7089
19	-	-	-	-	-	-	-	-	45.6773	66.4515
20	-	-	-	-	-	-	-	-	578.0634	227.0963
21	-	-	-	-	-	-	-	-	637.4181	178.7093
22	-	-	-	-	-	-	-	-	197.4190	277.4188
23	-	-	-	-	-	-	-	-	528.3860	248.3866
24	-	-	-	-	-	-	-	-	277.4188	193.5480
25	-	-	-	-	-	-	-	-	578.0634	250.3221
26	-	-	-	-	-	-	-	-	49.3547	81.2902
27	-	-	-	-	-	-	-	-	41.8709	221.9350
28	-	-	-	-	-	-	-	-	277.4188	94.8385
29	-	-	-	-	-	-	-	-	227.7415	193.5480
30	-	-	-	-	-	-	-	-	104.5159	123.2256
31	-	-	-	-	-	-	-	-	66.4515	41.8064
32	-	-	-	-	-	-	-	-	181.9351	307.7413
W (kg)	373.86	313.35	2507.94	1571.82	988.60	854.96	35,124.35	23,863.82	967,602.87	583,624.36
λ_1	144.41	124.96	80.82	56.90	662.58	551.58	11.11	7.90	172.65	91.37
$\lambda_2 - \lambda_1$	106.81	98.64	52.80	32.30	0	0	1.24	0.83	77.22	63.08
$\lambda_3 - \lambda_2$	321.22	236.12	19.55	10.31	738.76	445.03	0	0	60.98	29.13
$\lambda_4 - \lambda_3$	973.43	890.12	15.00	6.53	191.38	175.84	4.86	3.20	66.61	53.19

Table 5 provides detailed information on the extracted non-dominated solutions for scenarios sc_1 and sc_2 of MOSOP7. For the 25-bar truss, the weights of the non-dominated extracted solutions were 354.86 kg and 290.61 kg, respectively, for the sc_1 and sc_2 scenarios, resulting in a difference of approximately 22.10% in favor of the heavier structure. A difference of 68.00% was found between the final weights of the solutions extracted by the sc_1 and sc_2 scenarios of the 56-bar truss, i.e., 2141.14 kg and 1274.42 kg. For the 72-bar truss, the difference was 53.29% between the weights of the two extracted solutions, i.e., 768.83 kg vs. 501.54 kg. For the 120-bar truss, the weights of the extracted solutions were 38,356.29 vs. 19,948.30 kg, resulting in a difference of approximately 92.27% more for the heavier structure. Finally, for the 582-bar truss, the difference was 68.80% for the weights of 839,131.86 kg vs. 497,109.47 kg.

Table 5. Values obtained for the design variables and objective functions of the MTD solutions extracted from MOSOP7.

A_i (cm ²)	T25		T56		T72		T120		T582	
Scenario	sc_1	sc_2	sc_1	sc_2	sc_1	sc_2	sc_1	sc_2	sc_1	sc_2
D. Var.	SHAMODE-WO	SHAMODE-WO	MM-IPDE	MM-IPDE	SHAMODE-WO	SHAMODE-WO	MM-IPDE	SHAMODE	SHAMODE-WO	SHAMODE
1	5.1613	14.8387	10.9450	7.5308	3.6968	6.1328	139.8199	102.6235	216.1286	165.1610
2	19.3548	8.3871	12.4298	7.4917	15.0061	8.3677	36.3627	42.2049	651.6116	275.4833
3	16.7742	20.6451	8.9216	4.3630	5.4932	5.2807	53.3606	14.3509	212.2576	216.1286
4	14.8387	7.7419	-	-	4.9654	10.4095	140.0000	62.0051	359.9993	107.7417
5	3.2258	4.5161	-	-	15.0674	9.2059	106.9050	38.6835	200.6448	129.6772
6	14.8387	13.5484	-	-	18.2431	9.0692	16.0526	7.1106	231.6124	66.4515
7	14.1935	8.3871	-	-	16.0103	11.1653	4.4191	5.1719	1148.3848	257.4188
8	19.3548	19.3548	-	-	4.6311	2.7151	-	-	183.8706	275.4833
9	-	-	-	-	10.6598	6.0772	-	-	193.5480	138.7094
10	-	-	-	-	16.3891	11.6792	-	-	359.9993	94.8385
11	-	-	-	-	10.2074	8.0994	-	-	487.7410	156.7739
12	-	-	-	-	3.4620	2.7687	-	-	1148.3848	227.0963
13	-	-	-	-	24.7314	22.6756	-	-	637.4181	478.0636
14	-	-	-	-	18.2237	10.4959	-	-	221.9350	163.2255
15	-	-	-	-	8.6529	4.5785	-	-	703.2244	359.9993
16	-	-	-	-	7.2635	1.9435	-	-	637.4181	127.0963
17	-	-	-	-	-	-	-	-	528.3860	359.9993
18	-	-	-	-	-	-	-	-	248.3866	140.6449
19	-	-	-	-	-	-	-	-	307.7413	74.1934
20	-	-	-	-	-	-	-	-	276.7736	278.7091
21	-	-	-	-	-	-	-	-	57.0321	94.8385
22	-	-	-	-	-	-	-	-	123.2256	140.6449
23	-	-	-	-	-	-	-	-	278.7091	398.7089
24	-	-	-	-	-	-	-	-	117.4191	94.8385

Table 5. Cont.

A_i (cm ²)	T25		T56		T72		T120		T582	
Scenario	sc_1	sc_2	sc_1	sc_2	sc_1	sc_2	sc_1	sc_2	sc_1	sc_2
D. Var.	SHAMODE-WO	SHAMODE-WO	MM-IPDE	MM-IPDE	SHAMODE-WO	SHAMODE-WO	MM-IPDE	SHAMODE	SHAMODE-WO	SHAMODE
25	-	-	-	-	-	-	-	-	136.1288	187.7416
26	-	-	-	-	-	-	-	-	123.2256	145.8062
27	-	-	-	-	-	-	-	-	129.0320	159.3545
28	-	-	-	-	-	-	-	-	216.1286	94.8385
29	-	-	-	-	-	-	-	-	183.8706	81.2902
30	-	-	-	-	-	-	-	-	90.9676	74.1934
31	-	-	-	-	-	-	-	-	113.5482	49.0967
32	-	-	-	-	-	-	-	-	159.9997	136.1288
W (kg)	354.80	290.61	2141.14	1274.42	768.83	501.54	38,356.29	19,948.30	839,131.86	497,109.47
f_1 (Hz)	43.28	39.48	25.42	23.95	3.85	3.14	6.19	5.65	1.91	1.40
f_2 (Hz)	45.58	43.78	25.42	23.95	3.85	3.14	6.19	5.73	1.98	1.42
f_3 (Hz)	56.33	46.93	36.89	37.44	6.12	4.74	6.22	5.73	3.57	3.72
λ_1	152.94	96.26	77.59	49.29	482.02	311.58	11.33	6.66	159.83	118.99
λ_2	243.53	200.03	121.81	67.36	482.02	311.58	12.58	7.35	274.02	175.44
λ_3	610.10	357.44	135.50	74.86	1173.63	840.96	12.58	7.35	291.03	185.08

Tables A1–A4, provided in the Appendix, show the detailed information on the extracted non-dominated solutions for scenarios sc_1 and sc_2 of MOSOPs 2, 3, 5, and 6.

6.6. Analysis of Results

Observing the results from the extracted solutions of MOSOP1 (Figures 7–11 and Table 3) the 56-bar, 72-bar, and 120-bar trusses presented very low values for some differences between natural frequencies of vibrations, being more susceptible to problems related to overlapping their vibration modes. It is also observed that the solutions obtained with sc_2 provide considerably lighter structures than those of sc_1 (except for 56-bar, for which the same solution was extracted in both cases). At the same time, the other objectives present less significant variations.

Regarding the results found for MOSOP4 (Figures 12–16 and Table 4), 72-bar and 120-bar trusses have the smallest differences between successive critical load factors, which can intensify their instability and displacements. It is also noted that the 120-bar truss has the smallest values of $\lambda_1(x)$, which is more likely to have stability problems than the other trusses.

Analyzing the results concerning MOSOP7 (Figures 17–21 and Table 5), the extracted solutions of sc_2 provided lighter structural configurations without leading a significant impact on the other objective functions. Furthermore, the 120-bar truss presented the least stable truss among the analyzed structures concerning global stability.

Table 6 summarizes the weight of all non-dominated solutions extracted from the Pareto fronts of scenarios sc_1 and sc_2 . This table makes it possible to evaluate the impact of the other objective functions, such as the natural frequencies of vibration, the critical load factors, and the differences between some of these values on the first objective function, which is the structure’s weight. This table highlights in bold the maximum and minimum values of the weights among the seven MOSOPs and the percentage values of these differences. The minimum percentage difference refers to the 25-bar truss with the lowest weight of 308.16 kg (MOSOP 4) and the highest of 373.86 kg (MOSOP 6), equivalent to a percentage difference of 21.09%. On the other hand, the largest percentage difference of 289.73% occurred in the 56-bar truss with a minimum weight of 643.50 kg (MOSOP3) and a maximum of 2507.94 kg (MOSOP5). Both cases refer to extracted solutions from sc_1 . These analyses will help the DM adapt their preferences, for example, whether vibrational aspects will be prioritized over the structure’s weight or aspects related to stability will be more important, among other possibilities.

Table 6. Weights of extracted non-dominated solutions of all experiments (kg).

MOSOP	T25		T56		T72		T120		T582	
	sc ₁	sc ₂	sc ₁	sc ₂	sc ₁	sc ₂	sc ₁	sc ₂	sc ₁	sc ₂
1	310.62	276.97	1039.89	1039.89	754.86	576.96	29,054.60	19,863.97	804,249.40	441,471.98
2	354.78	323.68	2479.70	1726.74	931.34	817.84	32,850.85	24,505.25	905,978.93	691,222.55
3	321.84	278.88	643.50	643.50	822.17	510.03	32,372.67	20,992.16	862,839.71	436,577.63
4	373.86	313.35	2507.94	1571.82	988.60	854.96	35,124.35	23,863.82	967,602.87	583,624.36
5	360.01	310.69	2430.72	1457.44	1001.50	800.19	35,477.15	22,608.72	864,962.04	492,201.58
6	308.16	261.08	784.73	425.42	832.58	518.57	27,973.61	16,858.52	678,888.75	395,151.83
7	354.80	290.61	2141.14	1274.42	768.83	501.54	38,356.29	19,948.30	839,131.86	497,109.47
	21.09%	23.98%	289.73%	168.33%	32.67%	70.46%	37.11%	45.35%	42.53%	74.92%

Finally, an additional critical analysis is carried out due to some interesting results observed in the characteristics of the extracted solutions. For example, in MOSOP1, the second objective function, which is the difference between the frequencies f_1 and f_2 , must be maximized, and the values for 56-bar, 72-bar, and 582-bar are very close to 0 in both scenarios. Similarly, this occurs for the third objective function, concerning the difference between f_3 and f_2 for the 120-bar truss in both extraction scenarios. This is due to the structure’s characteristics, such as the symmetry of the bars and topology, which causes neighboring natural frequencies to have similar values. It is crucial for the DM to carefully consider adopting these extracted solutions given that if not managed effectively, it could potentially lead to undesirable situations, including the risk of structural collapse. Given the availability of other non-dominated solutions, the DMs can select different extraction preferences for these structures based on their understanding of the design’s requirements and the specified limits for the objective functions. Therefore, it is emphasized that when this occurs, the results of the MOSOPs analyzed in this paper illustrate the importance of this type of “warning” to the DM to extract alternative solutions, if applicable. Similar situations can be observed in other solutions obtained for other MOSOPs, also in terms of critical load factors.

6.7. Performance Indicators—Hypervolume (HV) and IGD+

After the MOSOPs in the analyzed trusses are solved, the algorithms’ performances are compared using two well-known indicators in the literature: HV, whose relative values were also presented and discussed in the previous sections, and IGD+.

Table 7 provides the percentage of non-dominated solutions provided by each algorithm and the ratios between each algorithm’s HV and the HV of the total set of non-dominated solutions (in parentheses). The values in bold in this table indicate the MOEA that contributed with the most non-dominated solutions in the unified PF. From the results presented in Table 7, it is possible to observe that MM-IPDE was the algorithm that provided more non-dominated solutions for the unified PFs of all trusses.

Tables 8–14 present the mean and standard deviation of the values obtained for HV and IGD+ from the independent executions of MOSOPs 1 to 7 in each truss. Regarding the HV, bigger values indicate better performances of the algorithms, while for the IGD+ smaller results designate better performances. The best values are highlighted in bold. The symbol (+) means that there is a statistically significant difference (p -value < 0.05) between the results of the algorithms compared to the one with the best performance according to the non-parametric Wilcoxon test.

Table 7. Percentage of non-dominated solutions provided by each algorithm and the ratios between each algorithm’s HV and the HV of the total set of non-dominated solutions (in parentheses).

MOSOP	Algorithm	T25	T56	T72	T120	T582
1	MM-IPDE	36.43 (0.8651)	39.81 (0.6382)	41.60 (0.7485)	39.48 (0.9601)	72.01 (0.9077)
	SHAMODE	34.84 (0.7849)	31.28 (0.9509)	31.15 (0.8390)	30.83 (0.1832)	12.83 (0.7036)
	SHAMODE-WO	28.73 (0.8498)	28.91 (0.8486)	21.25 (0.8468)	29.69 (0.2642)	15.16 (0.6580)
2	MM-IPDE	35.03 (0.9564)	28.49 (0.8763)	51.35 (0.8469)	39.29 (0.7961)	42.37 (0.9747)
	SHAMODE	31.73 (0.6061)	36.03 (0.9236)	27.43 (0.8717)	33.06 (0.8432)	25.79 (0.2716)
	SHAMODE-WO	33.24 (0.6056)	35.48 (0.9390)	21.22 (0.6928)	27.65 (0.9737)	31.84 (0.3406)
3	MM-IPDE	33.94 (0.7613)	40.30 (0.7185)	38.25 (0.6989)	41.42 (0.8989)	62.47 (0.8149)
	SHAMODE	34.89 (0.8459)	28.54 (0.7612)	33.33 (0.7995)	27.61 (0.5176)	14.65 (0.6767)
	SHAMODE-WO	31.17 (0.8441)	31.16 (0.8959)	28.42 (0.8355)	30.97 (0.6178)	22.88 (0.7884)
4	MM-IPDE	30.42 (0.8243)	28.70 (0.6042)	46.59 (0.8371)	41.30 (0.9470)	40.26 (0.9632)
	SHAMODE	33.05 (0.7069)	35.58 (0.9356)	32.72 (0.5534)	34.60 (0.6966)	28.04 (0.1261)
	SHAMODE-WO	36.53 (0.7553)	35.72 (0.8773)	20.69 (0.2645)	24.10 (0.6988)	31.70 (0.3306)
5	MM-IPDE	32.65 (0.9602)	30.29 (0.8447)	47.39 (0.8546)	41.93 (0.7457)	42.53 (0.9840)
	SHAMODE	31.31 (0.4831)	34.72 (0.9281)	29.90 (0.8437)	31.74 (0.9428)	28.59 (0.0854)
	SHAMODE-WO	36.04 (0.5168)	34.99 (0.9346)	22.71 (0.7121)	26.33 (0.8999)	28.88 (0.1707)
6	MM-IPDE	33.77 (0.8426)	41.16 (0.6453)	46.91 (0.9146)	37.28 (0.9219)	59.60 (0.7109)
	SHAMODE	36.73 (0.8433)	29.54 (0.8584)	24.43 (0.7664)	35.69 (0.6101)	18.80 (0.7109)
	SHAMODE-WO	29.50 (0.8272)	29.30 (0.8433)	28.66 (0.7757)	27.03 (0.3801)	21.60 (0.7109)
7	MM-IPDE	33.71 (0.9235)	38.16 (0.9509)	43.01 (0.9849)	50.30 (0.9791)	40.05 (0.9035)
	SHAMODE	31.97 (0.6723)	31.24 (0.9099)	22.93 (0.8825)	31.45 (0.9827)	30.45 (0.2394)
	SHAMODE-WO	34.32 (0.6723)	30.60 (0.9173)	34.06 (0.8648)	18.25 (0.9691)	29.50 (0.2319)

Table 8. Mean values and standard deviation (SD) of the results obtained for HV and IGD+ from the independent executions of MOSOP1.

Number of Bars	MM-IPDE		SHAMODE		SHAMODE-WO	
	Mean	SD	Mean	SD	Mean	SD
HV						
25	0.06849	0.01582	0.07462	0.02458	0.07195	0.02777
56	$3.5546 \times 10^{-13}(+)$	7.7277×10^{-14}	4.6955×10^{-13}	9.9883×10^{-14}	4.8235×10^{-13}	8.5249×10^{-14}
72	0.24389	0.03068	0.24318	0.04776	0.25383	0.03773
120	3.7414×10^{-13}	1.6780×10^{-13}	3.5029×10^{-13}	3.0102×10^{-14}	3.5353×10^{-13}	3.5352×10^{-14}
582	0.33236	0.07968	0.30646	0.06429	0.28673	0.05954
IGD+						
25	0.09448	0.01652	0.17654 (+)	0.05426	0.18683 (+)	0.05894
56	0.05068	0.01752	0.06282	0.02180	0.05516	0.02015
72	0.07193	0.00979	0.07288	0.01315	0.07222	0.01325
120	0.02684	0.00514	0.03268 (+)	0.00902	0.03018 (+)	0.00585
582	0.11368	0.04272	0.11479	0.02536	0.11803	0.03285

Table 9. Mean values and standard deviation (SD) of the results obtained for HV and IGD+ from the independent executions of MOSOP2.

Number of Bars	MM-IPDE		SHAMODE		SHAMODE-WO	
	Mean	SD	Mean	SD	Mean	SD
HV						
25	0.16173	0.00651	0.08679 (+)	0.01841	0.09068 (+)	0.01830
56	0.17462 (+)	0.02190	0.20324	0.01214	0.20436	0.01422
72	1.1255×10^{-12}	1.3393×10^{-13}	9.9229×10^{-13} (+)	1.7876×10^{-13}	9.7009×10^{-13} (+)	1.3212×10^{-13}
120	0.40913	0.07430	0.41571	0.07796	0.46354	0.10581
582	0.13261	0.06859	0.03323 (+)	0.01115	0.04300 (+)	0.01320
IGD+						
25	0.11630	0.01075	0.14272 (+)	0.03861	0.13556	0.03756
56	0.07845 (+)	0.01383	0.06795 (+)	0.00975	0.06093	0.00644
72	0.04109	0.01286	0.05550 (+)	0.01918	0.05685 (+)	0.01788
120	0.04220 (+)	0.00989	0.03301	0.01218	0.03060	0.01026
582	0.09697	0.05015	0.16957 (+)	0.02903	0.15280 (+)	0.02198

Table 10. Mean values and standard deviation (SD) of the results obtained for HV and IGD+ from the independent executions of MOSOP3.

Number of Bars	MM-IPDE		SHAMODE		SHAMODE-WO	
	Mean	SD	Mean	SD	Mean	SD
HV						
25	0.04072 (+)	0.00936	0.05887	0.02774	0.05523	0.02738
56	0.23312	0.03591	0.22096	0.05955	0.27748	0.10347
72	0.11459	0.02660	0.13047	0.02807	0.13088	0.02859
120	6.2191×10^{-13}	1.5094×10^{-13}	5.5836×10^{-13}	6.5117×10^{-14}	5.7339×10^{-13}	7.0279×10^{-14}
582	0.21841	0.04574	0.16308 (+)	0.04811	0.19451	0.04820
IGD+						
25	0.16269	0.02512	0.20308	0.12629	0.22604	0.13110
56	0.10500	0.01640	0.13456 (+)	0.03011	0.12231	0.03308
72	0.08741	0.01395	0.09313	0.01886	0.09115	0.01085
120	0.03952	0.00979	0.04382 (+)	0.00852	0.03821	0.00747
582	0.12890	0.02319	0.19376 (+)	0.03742	0.16669 (+)	0.04111

Table 11. Mean values and standard deviation (SD) of the results obtained for HV and IGD+ from the independent executions of MOSOP4.

Number of Bars	MM-IPDE		SHAMODE		SHAMODE-WO	
	Mean	SD	Mean	SD	Mean	SD
HV						
25	0.03217 (+)	0.00743	0.03455 (+)	0.01244	0.04165	0.01143
56	0.02441 (+)	0.00517	0.03844	0.00890	0.03666	0.00694
72	0.05365	0.01074	0.02338 (+)	0.01069	0.01280 (+)	0.00520
120	0.49518	0.14716	0.46922	0.09729	0.45157	0.09659
582	0.03144	0.01901	0.00439 (+)	0.00211	0.00696 (+)	0.00719
IGD+						
25	0.16389	0.01947	0.17649	0.06406	0.16256	0.06372
56	0.09480	0.01188	0.08827	0.01399	0.08699	0.00899
72	0.08726	0.01143	0.11821 (+)	0.02003	0.13368 (+)	0.01842
120	0.03583 (+)	0.00698	0.02617	0.00541	0.02798	0.00586
582	0.12124	0.04508	0.15910 (+)	0.02058	0.15172 (+)	0.02906

Table 12. Mean values and standard deviation (SD) of the results obtained for HV and IGD+ from the independent executions of MOSOP5.

Number of Bars	MM-IPDE		SHAMODE		SHAMODE-WO	
	Mean	SD	Mean	SD	Mean	SD
HV						
25	0.07751	0.00529	0.02534 (+)	0.01039	0.03012 (+)	0.00845
56	0.11661 (+)	0.00965	0.13300	0.00658	0.12820	0.00855
72	7.1324×10^{-13}	1.0568×10^{-13}	6.2953×10^{-13} (+)	1.6890×10^{-13}	6.0320×10^{-13} (+)	1.0961×10^{-13}
120	0.30210	0.05346	0.32763	0.07045	0.32857	0.07202
582	0.10763	0.08117	0.00701 (+)	0.00532	0.01428 (+)	0.01395
IGD+						
25	0.12272	0.01540	0.16375 (+)	0.04651	0.14101 (+)	0.02718
56	0.07241	0.00930	0.06530	0.01133	0.06660	0.00975
72	0.05362	0.00990	0.05656	0.01099	0.05502	0.01392
120	0.04485 (+)	0.00830	0.02971	0.00619	0.03334	0.00866
582	0.11105	0.05938	0.21423 (+)	0.02507	0.18923 (+)	0.02859

Table 13. Mean values and standard deviation (SD) of the results obtained for HV and IGD+ from the independent executions of MOSOP6.

Number of Bars	MM-IPDE		SHAMODE		SHAMODE-WO	
	Mean	SD	Mean	SD	Mean	SD
HV						
25	0.04146 (+)	0.01238	0.05018	0.02381	0.05039	0.02047
56	2.7391×10^{-13} (+)	6.6070×10^{-14}	3.5832×10^{-13}	7.8220×10^{-14}	3.2769×10^{-13}	9.0439×10^{-14}
72	0.16048	0.03350	0.14607	0.02555	0.15213	0.02226
120	4.4687×10^{-13}	2.6312×10^{-13}	3.3899×10^{-13}	1.6413×10^{-13}	3.0796×10^{-13}	3.5778×10^{-14}
582	0.21218	0.06466	0.17931	0.05733	0.17988	0.06640
IGD+						
25	0.09980	0.01776	0.17156 (+)	0.04548	0.16210 (+)	0.04079
56	0.05216	0.02338	0.07800 (+)	0.01850	0.08670 (+)	0.01862
72	0.08697	0.01797	0.09482	0.01780	0.09096	0.01520
120	0.04265	0.00890	0.03879	0.00784	0.04465 (+)	0.01003
582	0.10246	0.02764	0.14331 (+)	0.03724	0.14669 (+)	0.05190

Table 14. Mean values and standard deviation (SD) of the results obtained for HV and IGD+ from the independent executions of MOSOP7.

Number of Bars	MM-IPDE		SHAMODE		SHAMODE-WO	
	Mean	SD	Mean	SD	Mean	SD
HV						
25	0.16068	0.00908	0.10341 (+)	0.01986	0.11562 (+)	0.01203
56	0.17052	0.01014	0.15620 (+)	0.00795	0.15065 (+)	0.01302
72	0.29019	0.01403	0.25604 (+)	0.03073	0.25814 (+)	0.02457
120	0.63033	0.00992	0.62332	0.01329	0.61440 (+)	0.01148
582	0.03429	0.02940	0.00814 (+)	0.00624	0.00994 (+)	0.00512
IGD+						
25	0.12380 (+)	0.01913	0.12240 (+)	0.02984	0.10361	0.02047
56	0.06436	0.01258	0.08525 (+)	0.01606	0.08577 (+)	0.01760
72	0.05134	0.00950	0.06074	0.02180	0.05060	0.01091
120	0.01208	0.00363	0.01386 (+)	0.00301	0.01409 (+)	0.00214
582	0.20772	0.07871	0.24990	0.06891	0.22496	0.04277

6.8. Performance Profiles

As mentioned in Section 4, the area under the performance profile curve $\rho_s(\tau)$ is an indicator of the general performance of the algorithm s in solving the problem set P (number of problems $n_p = 35$, as there are seven MOSOPs for each of the five trusses). The larger the area, the better the performance of the analyzed algorithm.

Figures 22 and 23 represent the PPs referring to the HV and IGD+ values, respectively, presented in Tables 8–14. Each PP is related to the results of its performance indicator in solving the respective MOSOP for all analyzed trusses. The areas under the curves (normalized by the largest of them) are in the description of each figure, in the order MM-IPDE, SHAMODE, and SHAMODE-WO, indicating the performance of the algorithms in the resolution of the problems.

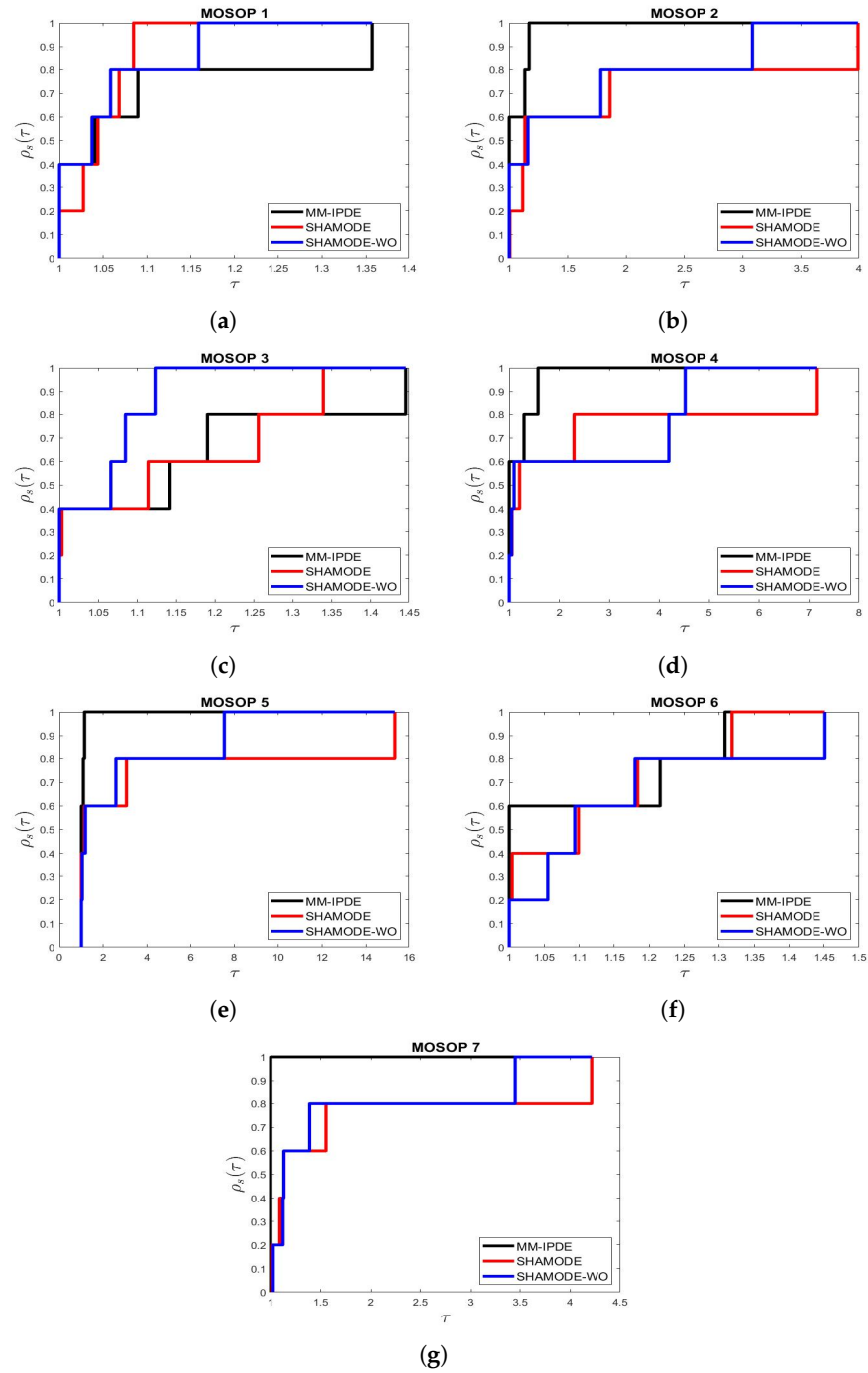


Figure 22. Performance profiles referring to the HV values presented in Tables 8–14. The areas below the curves (normalized by the largest of them) are in the description of each figure, in this order: MM-IPDE, SHAMODE, and SHAMODE-WO: (a) 0.8312; 1.0000; 0.9802; (b) 1.0000; 0.7402; 0.8140; (c) 0.7418; 0.7757; 1.0000; (d) 1.0000; 0.7713; 0.8001; (e) 1.0000; 0.7719; 0.8867; (f) 1.0000; 0.9533; 0.8525; and (g) 1.0000; 0.7508; 0.8057.

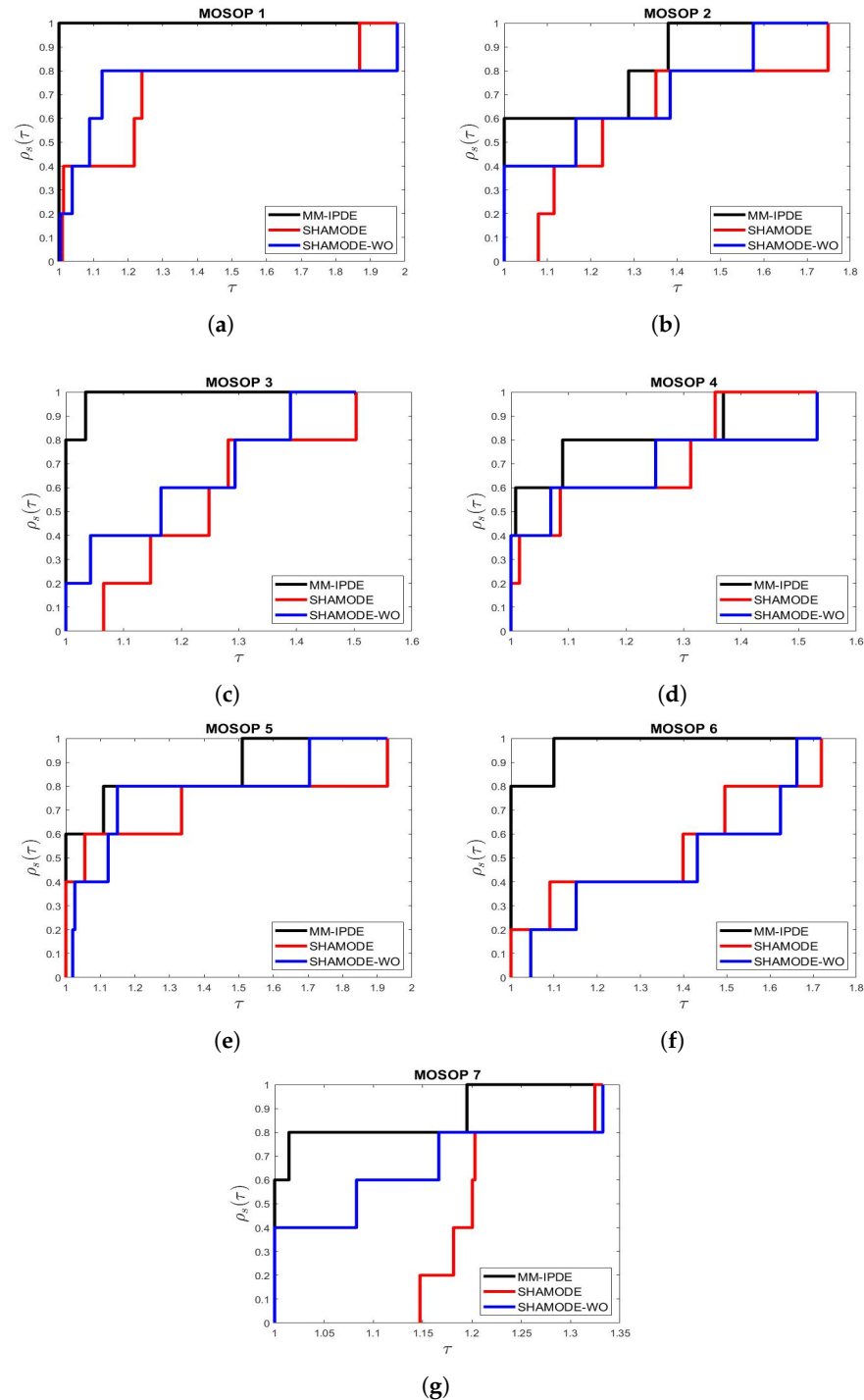


Figure 23. Performance profiles referring to the IGD+ values presented in Tables 8–14. The areas below the curves (normalized by the largest of them) are in the description of each figure, in this order: MM-IPDE, SHAMODE, and SHAMODE-WO: (a) 1.0000; 0.7241; 0.7478; (b) 1.0000; 0.7225; 0.8511; (c) 1.0000; 0.5120; 0.6551; (d) 1.0000; 0.8631; 0.8242; (e) 1.0000; 0.8262; 0.9000; (f) 1.0000; 0.5412; 0.4806; and (g) 1.0000; 0.4172; 0.7437.

Analyzing the PPs from Figure 22, related to the HV, it is possible to observe that according to the normalized areas under the PPs, MM-IPDE had the best performances in MOSOPs 2, 4, 5, 6, and 7, while SHAMODE was the best for MOSOP1 and SHAMODE-WO for MOSOP3. Regarding the IGD+ indicator, MM-IPDE had the greatest areas and, therefore, the best performance in all the analyzed MOSOPs. Concerning the definition

of the most efficient algorithm for a given optimization problem, the difference between results provided by different metrics has already been mentioned by Carvalho et al. in [1].

To evaluate according to each metric the performance of the meta-heuristics in solving the total set of proposed MOSOPs, Figure 24 represents the general performance profiles related to the HV and IGD+ values obtained in this study. To create these profiles, the areas under the profile curves of each MOSOP (indicated in Figure 22 for HV and Figure 23 for IGD+) were considered as the performance metric $t_{p,s}$. Thus, it was possible to outline the general performance profiles of each algorithm for both HV (Figure 24a) and IGD+ (Figure 24b). Again, the areas below the curves (normalized by the largest of them) are in the graph description in the order: MM-IPDE, SHAMODE, and SHAMODE-WO.

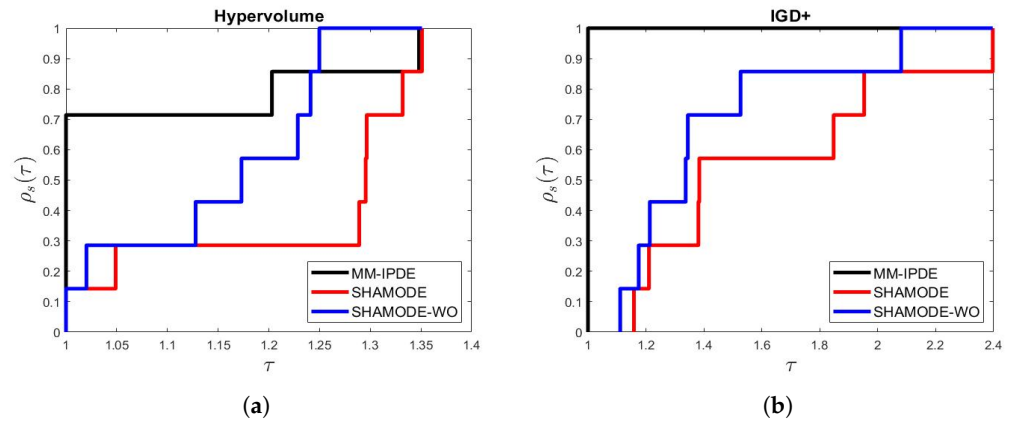


Figure 24. General performance profiles referring to the HV and IGD+. The areas below the curves (normalized by the largest of them) are in the description of each figure, in this order: MM-IPDE, SHAMODE, and SHAMODE-WO: (a) 1.0000; 0.4428; 0.7432; (b) 1.0000; 0.5570; 0.7148.

It is observed that the general performance profiles of both metrics point to MM-IPDE as the algorithm with the best overall performance in solving the MOSOPs for the proposed trusses, followed by SHAMODE-WO and, with the worst performance, SHAMODE.

Finally, to present a definitive conclusion about the algorithms that best performed in the MOSOPs of this study, Figure 25 displays the global performance profiles referring to the merged analysis of HV and IGD+. To make this analysis and obtain such profiles, the areas under the profile curves of each MOSOP were used again (Figure 22 for HV and Figure 23 for IGD+) as the performance metric $t_{p,s}$. This time, however, the areas related to HV and those obtained from the IGD+ graphs were analyzed together, providing a global perspective on the algorithm’s performance in terms of both metrics.

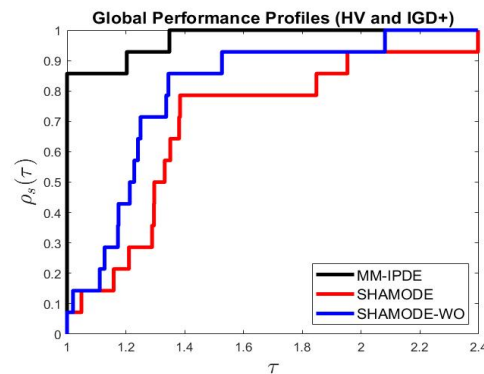


Figure 25. Global performance profiles referring to the merged analysis of HV and IGD+. The areas below the curves (normalized by the largest of them) are in the description of each figure, in this order: MM-IPDE, SHAMODE, and SHAMODE-WO: 1.0000; 0.7162; 0.8275.

Therefore, it can be seen in Figure 25 that, as expected, MM-IPDE presented the best overall performance in solving the MOSOPs for the proposed trusses. SHAMODE-WO provides the second-best overall performance, indicating that adding the WOA spiral motion operator to the original algorithm improved results. The merged analysis also pointed out SHAMODE as the algorithm with the worst overall performance in solving the optimization problems addressed in this work.

7. Conclusions

The solution of MOSOPs with objective functions and constraints related to natural frequencies of vibration and critical load factors is important in avoiding the effect of resonance in the dynamic behavior of structures and guaranteeing their global stability. This helps designers and engineers find structural solutions that meet their design requirements concerning weight, safety, usability, and user comfort.

The main objective established for this paper referred to the formulation and application of MOSOPs in spatial trusses, involving objectives and constraints related to dynamic and global stability aspects. It is possible to conclude that this objective was achieved with the solution of MOSOPs with four to seven objective functions, applied in five different trusses, which provided a large number of non-dominated solutions, allowing the DM to choose the structural configurations that best meet their needs and intentions. Furthermore, one innovative aspect of this study was the consideration of objective functions aiming to maximize the differences between the natural frequencies of vibration and between the critical load factors of the structures, enabling the designer to find solutions that are less susceptible to problems related to resonance between their vibration modes and the overlapping of their buckling modes.

The proposed MOSOPs are classified as many-objective structural optimization problems since they have more than three objective functions. Formulating structural optimization problems as many-objective problems can provide DMs with a more complete understanding of the problem, enabling them to make more robust and reliable decisions. As these problems have not received the expected attention in the literature, this study is a significant step forward in addressing this gap. Furthermore, the MTD method proved to be very efficient in finding structures that met the DM's criteria according to the importance (weight) attributed to each objective function. Another objective achieved by this paper was to compare the performances of the three state-of-the-art DE-based MOEAs used to solve the proposed MOSOPs.

As future work, we expect to propose new MOSOPs considering the inclusion of more objective functions, such as aspects related to critical loads in post-buckling behavior, including inelastic characteristics of materials, with applications in the optimization of trusses and shallow domes. Finally, we expect to apply machine learning algorithms to minimize the high computational costs required to evaluate the objective functions and constraints.

Author Contributions: Conceptualization, methodology, software, validation, formal analysis, investigation, resources, data curation, writing—original draft preparation, writing—review and editing, visualization, supervision, project administration, funding acquisition, J.M.P.V., J.P.G.C., D.E.C.V., É.C.R.C., P.H.H., and A.C.C.L. All authors have read and agreed to the published version of the manuscript.

Funding: The authors thank the Coordenação de Aperfeiçoamento de Pessoal de Nível Superior—CAPES (Finance Code 001), the Conselho Nacional de Desenvolvimento Científico e Tecnológico—CNPq (Grants 308105/2021-4 and 303221/2022-4), and the Fundação de Amparo à Pesquisa do Estado de Minas Gerais—FAPEMIG (Grants TEC PPM-00174-18, APQ-00869-22, and APQ 00408-21) for their supports.

Data Availability Statement: Data will be made available on request.

Conflicts of Interest: The authors declare that they have no known competing financial interests or personal relationships that could have appeared to influence the work reported in this paper.

Appendix A

Table A1. Values obtained for the design variables and objective functions of the MTD solutions extracted from MOSOP2.

A_i (cm ²)	T25		T56		T72		T120		T582	
Scenario	sc_1	sc_2	sc_1	sc_2	sc_1	sc_2	sc_1	sc_2	sc_1	sc_2
D. Var.	SHAMODE	SHAMODE	SHAMODE-WO	SHAMODE	MM-IPDE	MM-IPDE	SHAMODE	SHAMODE-WO	MM-IPDE	SHAMODE
1	14.1935	6.4516	11.5485	9.4270	12.2294	9.3759	138.8009	122.0141	337.4187	66.4515
2	13.5484	10.3226	13.9002	9.1491	21.8062	22.2072	60.9155	61.4018	337.4187	578.0634
3	14.1935	15.4838	11.6346	7.2334	19.8998	9.8162	18.8396	20.8802	337.4187	478.0636
4	10.9677	12.9032	-	-	2.9691	3.5996	124.9358	83.7655	337.4187	100.6450
5	12.9032	8.3871	-	-	22.6512	11.1628	70.4793	31.0734	337.4187	178.7093
6	20.6451	20.6451	-	-	16.6328	14.6773	6.5921	3.4781	337.4187	210.9673
7	12.9032	10.9677	-	-	14.1773	14.2252	5.4838	7.1942	337.4187	275.4833
8	18.0645	16.1290	-	-	0.8066	0.9947	-	-	359.9993	90.9676
9	-	-	-	-	23.3475	24.8685	-	-	528.3860	118.0643
10	-	-	-	-	17.5254	19.7926	-	-	337.4187	94.8385
11	-	-	-	-	25.8060	14.6551	-	-	337.4187	221.9350
12	-	-	-	-	2.1132	2.5302	-	-	1045.1592	210.9673
13	-	-	-	-	24.6398	25.2552	-	-	337.4187	170.9674
14	-	-	-	-	17.0898	16.6418	-	-	193.5480	578.0634
15	-	-	-	-	13.6292	4.8607	-	-	337.4187	275.4833
16	-	-	-	-	0.6516	0.8076	-	-	337.4187	200.6448
17	-	-	-	-	-	-	-	-	864.5144	537.4183
18	-	-	-	-	-	-	-	-	68.3870	301.2897
19	-	-	-	-	-	-	-	-	66.4515	200.6448
20	-	-	-	-	-	-	-	-	337.4187	1148.3848
21	-	-	-	-	-	-	-	-	337.4187	49.3547
22	-	-	-	-	-	-	-	-	334.1929	366.4509
23	-	-	-	-	-	-	-	-	337.4187	197.4190
24	-	-	-	-	-	-	-	-	145.8062	307.7413
25	-	-	-	-	-	-	-	-	337.4187	66.4515
26	-	-	-	-	-	-	-	-	337.4187	178.7093
27	-	-	-	-	-	-	-	-	110.3224	187.7416
28	-	-	-	-	-	-	-	-	226.4512	94.1934
29	-	-	-	-	-	-	-	-	337.4187	221.9350
30	-	-	-	-	-	-	-	-	337.4187	305.8058
31	-	-	-	-	-	-	-	-	337.4187	58.8386
32	-	-	-	-	-	-	-	-	337.4187	53.2257
W (kg)	354.78	323.68	2479.70	1726.74	931.34	817.84	32,850.85	24,505.25	905,978.93	691,222.55
λ_1	140.38	120.82	84.67	60.77	710.35	631.19	10.64	8.26	161.59	114.23
$\lambda_2 - \lambda_1$	107.27	118.21	59.60	39.34	0	0	1.17	0.86	82.75	84.60
$\lambda_3 - \lambda_2$	384.07	305.76	16.39	9.85	829.43	624.33	0	0	101.29	51.02

Table A2. Values obtained for the design variables and objective functions of the MTD solutions extracted from MOSOP3.

A_i (cm ²)	T25		T56		T72		T120		T582	
Scenario	sc_1	sc_2	sc_1	sc_2	sc_1	sc_2	sc_1	sc_2	sc_1	sc_2
D. Var.	SHAMODE-WO	SHAMODE	MM-IPDE	MM-IPDE	MM-IPDE	MM-IPDE	MM-IPDE	SHAMODE-WO	MM-IPDE	MM-IPDE
1	3.2258	1.9355	3.5057	3.5057	11.9521	4.1954	83.9015	51.7107	334.1929	127.0965
2	5.8064	2.5806	2.7481	2.7481	9.4987	9.8330	33.6933	44.5132	250.3221	487.7410
3	19.3548	19.3548	3.1274	3.1274	4.6008	6.0389	18.5951	14.1340	1264.5136	227.7415
4	18.0645	7.0968	-	-	14.3302	7.1399	140.0000	85.6471	703.2244	337.4187
5	7.7419	1.2903	-	-	17.6678	8.9800	70.7834	38.3752	83.8708	66.4515
6	15.4838	10.9677	-	-	24.1404	16.2796	28.0943	94.8385	39.7419	39.7419
7	16.1290	18.0645	-	-	13.6265	6.0383	15.5746	11.7173	589.6762	441.9346
8	16.1290	16.1290	-	-	18.4797	6.7039	-	-	129.6772	192.2577
9	-	-	-	-	24.2875	11.0618	-	-	337.4187	39.7419
10	-	-	-	-	19.2344	8.3536	-	-	322.5800	276.7736
11	-	-	-	-	1.2409	1.1206	-	-	159.3545	49.3547
12	-	-	-	-	6.7649	1.5663	-	-	337.4187	305.8058
13	-	-	-	-	12.4538	9.0592	-	-	231.6124	275.4833
14	-	-	-	-	14.7725	10.7972	-	-	212.2576	144.5158
15	-	-	-	-	11.6230	4.5120	-	-	1045.1592	181.9351
16	-	-	-	-	8.8315	11.9779	-	-	399.9992	159.3545
17	-	-	-	-	-	-	-	-	399.9992	307.7413
18	-	-	-	-	-	-	-	-	201.2899	136.1288
19	-	-	-	-	-	-	-	-	57.0967	39.7419
20	-	-	-	-	-	-	-	-	337.4187	337.4187
21	-	-	-	-	-	-	-	-	39.7419	39.7419
22	-	-	-	-	-	-	-	-	39.7419	39.7419
23	-	-	-	-	-	-	-	-	806.4500	337.4187
24	-	-	-	-	-	-	-	-	81.2902	49.6128
25	-	-	-	-	-	-	-	-	39.7419	39.7419
26	-	-	-	-	-	-	-	-	193.5480	206.4512
27	-	-	-	-	-	-	-	-	45.6773	101.9353
28	-	-	-	-	-	-	-	-	197.4190	129.6772
29	-	-	-	-	-	-	-	-	170.9674	58.9031
30	-	-	-	-	-	-	-	-	183.8706	192.2577
31	-	-	-	-	-	-	-	-	76.1289	206.4512
32	-	-	-	-	-	-	-	-	129.0320	39.7419
W (kg)	321.84	278.88	643.50	643.50	822.17	510.03	32,372.67	20,992.16	862,839.71	436,577.63
f_1 (Hz)	38.25	31.57	25.78	25.78	3.68	2.92	5.52	4.85	1.60	1.53
$f_2 - f_1$ (Hz)	7.06	14.17	0	0	0	0	0.12	0.11	0.06	0.06
$f_3 - f_2$ (Hz)	10.46	6.68	10.04	10.04	2.33	1.81	0	0	2.34	2.57
$f_4 - f_3$ (Hz)	20.60	16.90	2.81	2.81	4.20	2.97	0.41	0.38	0.72	0.73

Table A3. Values obtained for the design variables and objective functions of the MTD solutions extracted from MOSOP5.

A_i (cm ²)	T25		T56		T72		T120		T582	
Scenario	sc_1	sc_2	sc_1	sc_2	sc_1	sc_2	sc_1	sc_2	sc_1	sc_2
D. Var.	SHAMODE	SHAMODE	SHAMODE-WO	SHAMODE-WO	MM-IPDE	SHAMODE	SHAMODE	SHAMODE-WO	SHAMODE-WO	MM-IPDE
1	5.8064	5.8064	11.9686	7.1438	9.6969	12.7043	139.9829	113.3343	478.0636	231.6124
2	20.6451	11.6129	13.1954	7.1243	22.6366	12.7204	47.2919	55.1637	68.3870	107.7417
3	15.4838	18.0645	11.1155	7.1993	12.7492	6.8221	40.2536	10.7307	250.3221	221.9350
4	16.7742	9.6774	-	-	5.4101	5.0471	138.9559	70.1522	1148.3850	210.9673
5	1.9355	3.8710	-	-	24.9356	16.8832	63.1236	46.2733	322.5800	107.7417
6	18.0645	19.3548	-	-	18.0818	13.9176	10.2484	10.6235	167.0964	197.4190
7	13.5484	8.3871	-	-	23.3592	14.3682	9.3118	6.0279	1387.0940	278.7091
8	16.7742	16.7742	-	-	1.9442	3.9174	-	-	189.6770	138.7094
9	-	-	-	-	21.6753	25.8036	-	-	227.7415	176.1287
10	-	-	-	-	22.6436	19.2670	-	-	90.96756	138.7094
11	-	-	-	-	15.5379	10.7139	-	-	123.2256	226.4512
12	-	-	-	-	1.9781	9.9969	-	-	537.4183	278.7091
13	-	-	-	-	24.4922	24.8591	-	-	1045.1590	178.7093
14	-	-	-	-	20.3056	20.6456	-	-	250.3221	210.9673
15	-	-	-	-	15.1115	8.1389	-	-	637.4181	192.2577
16	-	-	-	-	4.8008	0.9820	-	-	366.4509	117.4191
17	-	-	-	-	-	-	-	-	1264.5140	210.9673
18	-	-	-	-	-	-	-	-	159.9997	192.2577
19	-	-	-	-	-	-	-	-	49.0967	278.7091
20	-	-	-	-	-	-	-	-	169.0519	276.7736
21	-	-	-	-	-	-	-	-	115.4836	76.12888
22	-	-	-	-	-	-	-	-	110.3224	248.3866
23	-	-	-	-	-	-	-	-	277.4188	163.2255
24	-	-	-	-	-	-	-	-	216.1286	210.9673
25	-	-	-	-	-	-	-	-	87.0966	117.4191
26	-	-	-	-	-	-	-	-	94.8385	83.8708
27	-	-	-	-	-	-	-	-	90.9676	94.8385
28	-	-	-	-	-	-	-	-	62.6450	104.5159
29	-	-	-	-	-	-	-	-	92.9030	178.7093
30	-	-	-	-	-	-	-	-	108.3869	189.677
31	-	-	-	-	-	-	-	-	275.4833	250.3221
32	-	-	-	-	-	-	-	-	257.4188	129.0320
W (kg)	360.01	310.69	2430.72	1457.44	1001.50	800.19	35,477.15	22,608.72	864,962.04	492,201.58
λ_1	148.92	101.70	83.39	46.84	720.81	621.69	11.16	7.42	139.30	78.55
λ_2	253.30	227.17	142.50	87.76	720.81	621.69	12.39	8.19	241.14	132.47
λ_3	596.21	512.42	157.59	94.86	1817.19	1165.98	12.39	8.19	381.45	169.30
$\lambda_2 - \lambda_1$	106.37	125.48	59.12	40.91	0	0	1.23	0.77	101.84	53.92
$\lambda_3 - \lambda_2$	340.91	285.24	15.09	7.11	1096.37	544.29	0	0	140.31	36.84

Table A4. Values obtained for the design variables and objective functions of the MTD solutions extracted from MOSOP6.

A_i (cm ²)	T25		T56		T72		T120		T582	
Scenario	sc_1	sc_2	sc_1	sc_2	sc_1	sc_2	sc_1	sc_2	sc_1	sc_2
D. Var.	SHAMODE	SHAMODE	SHAMODE	SHAMODE	SHAMODE	SHAMODE-WO	SHAMODE-WO	SHAMODE	MM-IPDE	MM-IPDE
1	1.9355	3.8710	3.9666	2.0332	3.5125	5.9587	83.3357	47.0608	41.8064	39.7419
2	5.8064	3.2258	3.8622	2.2808	9.5892	5.6675	27.9777	39.6662	651.6116	337.4187
3	19.3548	19.3548	3.7546	2.0176	15.7317	6.0512	30.4049	24.4641	110.3224	110.3224
4	3.8710	1.9355	-	-	6.5686	5.4587	86.1556	54.4415	651.6116	226.4512
5	3.8710	7.0968	-	-	8.0164	2.9947	69.8433	44.2815	334.1929	337.4187
6	14.1935	6.4516	-	-	20.4860	12.2111	30.6347	11.2129	231.6124	39.7419
7	18.0645	16.7742	-	-	0.7670	4.1211	33.2887	155.4836	155.4836	159.3545
8	16.7742	18.0645	-	-	11.5959	2.6549	-	-	227.0963	123.2256
9	-	-	-	-	20.3694	12.7197	-	-	39.7419	94.8385
10	-	-	-	-	21.2489	14.6734	-	-	399.9992	305.8058
11	-	-	-	-	8.8329	2.8922	-	-	637.4181	85.8063
12	-	-	-	-	13.3486	1.4531	-	-	864.5144	337.4187
13	-	-	-	-	16.5293	12.3645	-	-	216.1286	193.5480
14	-	-	-	-	24.0254	20.4339	-	-	129.0320	127.0965
15	-	-	-	-	11.0863	1.0462	-	-	305.8058	301.2897
16	-	-	-	-	2.1501	1.6375	-	-	637.4181	64.5160
17	-	-	-	-	-	-	-	-	589.6762	337.4187
18	-	-	-	-	-	-	-	-	159.3545	159.3545
19	-	-	-	-	-	-	-	-	39.7419	39.7419
20	-	-	-	-	-	-	-	-	578.0634	307.7413
21	-	-	-	-	-	-	-	-	39.7419	57.0321
22	-	-	-	-	-	-	-	-	39.7419	39.7419
23	-	-	-	-	-	-	-	-	337.4187	305.8058
24	-	-	-	-	-	-	-	-	39.7419	39.7419
25	-	-	-	-	-	-	-	-	39.7419	39.7419
26	-	-	-	-	-	-	-	-	149.6771	90.9676
27	-	-	-	-	-	-	-	-	94.1934	39.7419
28	-	-	-	-	-	-	-	-	75.4837	104.5159
29	-	-	-	-	-	-	-	-	212.2576	39.7419
30	-	-	-	-	-	-	-	-	189.6770	178.7093
31	-	-	-	-	-	-	-	-	189.6770	94.8385
32	-	-	-	-	-	-	-	-	76.1289	227.7415
W (kg)	308.16	261.08	784.73	425.42	832.58	518.57	27,973.61	16,858.52	678,888.75	395,151.83
f_1 (Hz)	38.44	33.39	26.08	26.18	3.83	3.09	5.58	4.69	1.62	1.47
f_2 (Hz)	46.32	44.31	26.08	26.18	3.83	3.09	5.70	4.79	1.70	1.54
f_3 (Hz)	57.27	49.68	36.65	36.43	6.68	5.58	5.70	4.79	4.20	3.77
$f_2 - f_1$ (Hz)	7.88	10.92	0	0	0	0	0.11	0.10	0.09	0.07
$f_3 - f_2$ (Hz)	10.95	5.37	10.58	10.26	2.84	2.49	0	0	2.50	2.23

References

1. Carvalho, J.P.G.; Carvalho, É.C.C.; Vargas, D.E.; Hallak, P.H.; Lima, B.S.; Lemonge, A.C. Multi-objective optimum design of truss structures using differential evolution algorithms. *Comput. Struct.* **2021**, *252*, 106544. [[CrossRef](#)]
2. Lemonge, A.C.; Carvalho, J.P.; Hallak, P.H.; Vargas, D.E. Multi-objective truss structural optimization considering natural frequencies of vibration and global stability. *Expert Syst. Appl.* **2021**, *165*, 113777. [[CrossRef](#)]
3. Storn, R.; Price, K. *Differential Evolution A Simple and Efficient Adaptive Scheme for Global Optimization over Continuous Spaces*; Tech. Rep. 95-012; University of California: Berkeley, CA, USA, 1995.
4. Panagant, N.; Bureerat, S.; Tai, K. A novel self-adaptive hybrid multi-objective meta-heuristic for reliability design of trusses with simultaneous topology, shape and sizing optimisation design variables. *Struct. Multidiscip. Optim.* **2019**, *60*, 1937–1955. [[CrossRef](#)]
5. Wansasueb, K.; Pholdee, N.; Panagant, N.; Bureerat, S. Multiobjective meta-heuristic with iterative parameter distribution estimation for aeroelastic design of an aircraft wing. *Eng. Comput.* **2020**, *38*, 695–713. [[CrossRef](#)]
6. Carvalho, J.P.G.; Vargas, D.E.; Jacob, B.P.; Lima, B.S.; Hallak, P.H.; Lemonge, A.C. Multi-objective structural optimization for the automatic member grouping of truss structures using evolutionary algorithms. *Comput. Struct.* **2024**, *292*, 107230. [[CrossRef](#)]
7. Resende, C.; Martha, L.F.; Lemonge, A.; Hallak, P.; Carvalho, J.; Motta, J. Automatic Column Grouping of 3D Steel Frames via Multi-Objective Structural Optimization. *Buildings* **2024**, *14*, 191. [[CrossRef](#)]
8. Resende, C.; Martha, L.F.; Lemonge, A.; Hallak, P.; Carvalho, J.; Motta, J. Multi-objective structural optimization of spatial steel frames with column orientation and bracing system as design variables. *Adv. Comput. Des.* **2023**, *8*, 327.
9. Parreiras, R.; Vasconcelos, J. Decision making in multiobjective optimization aided by the multicriteria tournament decision method. *Nonlinear Anal. Theory Methods Appl.* **2009**, *71*, 191–198. [[CrossRef](#)]
10. Angelo, J.S.; Bernardino, H.S.; Barbosa, H.J. Ant colony approaches for multiobjective structural optimization problems with a cardinality constraint. *Adv. Eng. Softw.* **2015**, *80*, 101–115. [[CrossRef](#)]
11. Greiner, D.; Winter, G.; Emperador, J.M.; Galván, B. Gray coding in evolutionary multicriteria optimization: Application in frame structural optimum design. In Proceedings of the International Conference on Evolutionary Multi-Criterion Optimization, Guanajuato, Mexico, 9–11 March 2005; Springer: Berlin/Heidelberg, Germany, 2005; pp. 576–591.
12. Greiner, D.; Galván, B.; Emperador, J.M.; Méndez, M.; Winter, G. Introducing reference point using g-dominance in optimum design considering uncertainties: An application in structural engineering. In Proceedings of the International Conference on Evolutionary Multi-Criterion Optimization, Ouro Preto, Brazil, 5–8 April 2011; Springer: Berlin/Heidelberg, Germany, 2011; pp. 389–403.
13. Noilubla, N.; Bureerat, S. Simultaneous topology, shape and sizing optimisation of a three-dimensional slender truss tower using multiobjective evolutionary algorithms. *Comput. Struct.* **2011**, *89*, 2531–2538. [[CrossRef](#)]
14. Su, R.; Wang, X.; Gui, L.; Fan, Z. Multi-objective topology and sizing optimization of truss structures based on adaptive multi-island search strategy. *Struct. Multidiscip. Optim.* **2011**, *43*, 275–286. [[CrossRef](#)]
15. Vo-Duy, T.; Duong-Gia, D.; Ho-Huu, V.; Nguyen-Thoi, T. An Effective Couple Method for Reliability-Based Multi-Objective Optimization of Truss Structures with Static and Dynamic Constraints. *Int. J. Comput. Methods* **2020**, *17*, 1950016. [[CrossRef](#)]
16. Kumar, S.; Tejani, G.G.; Pholdee, N.; Bureerat, S.; Mehta, P. Hybrid Heat Transfer Search and Passing Vehicle Search optimizer for multi-objective structural optimization. *Knowl.-Based Syst.* **2020**, *212*, 106556. [[CrossRef](#)]
17. Kaveh, A.; Laknejadi, K. A novel hybrid charge system search and particle swarm optimization method for multi-objective optimization. *Expert Syst. Appl.* **2011**, *38*, 15475–15488. [[CrossRef](#)]
18. Richardson, J.N.; Adriaenssens, S.; Bouillard, P.; Coelho, R.F. Multiobjective topology optimization of truss structures with kinematic stability repair. *Struct. Multidiscip. Optim.* **2012**, *46*, 513–532. [[CrossRef](#)]
19. Kaveh, A.; Laknejadi, K. A hybrid evolutionary graph-based multi-objective algorithm for layout optimization of truss structures. *Acta Mech.* **2013**, *224*, 343–364. [[CrossRef](#)]
20. Xie, L.; Tang, H.; Hu, C.; Xue, S. An adaptive multi-objective immune algorithm for optimal design of truss structures. *J. Asian Archit. Build. Eng.* **2016**, *15*, 557–564. [[CrossRef](#)]
21. Kaveh, A.; Bakhshpoori, T. An efficient multi-objective cuckoo search algorithm for design optimization. *Adv. Comput. Des.* **2016**, *1*, 87–103. [[CrossRef](#)]
22. Tejani, G.G.; Pholdee, N.; Bureerat, S.; Prayogo, D. Multiobjective adaptive symbiotic organisms search for truss optimization problems. *Knowl.-Based Syst.* **2018**, *161*, 398–414. [[CrossRef](#)]
23. Vargas, D.E.; Lemonge, A.C.; Barbosa, H.J.; Bernardino, H.S. Differential evolution with the adaptive penalty method for structural multi-objective optimization. *Optim. Eng.* **2019**, *20*, 65–88. [[CrossRef](#)]
24. Kaveh, A.; Mahdavi, V.R. Multi-objective colliding bodies optimization algorithm for design of trusses. *J. Comput. Des. Eng.* **2019**, *6*, 49–59. [[CrossRef](#)]
25. Tejani, G.G.; Pholdee, N.; Bureerat, S.; Prayogo, D.; Gandomi, A.H. Structural optimization using multi-objective modified adaptive symbiotic organisms search. *Expert Syst. Appl.* **2019**, *125*, 425–441. [[CrossRef](#)]

26. Tejani, G.G.; Kumar, S.; Gandomi, A.H. Multi-objective heat transfer search algorithm for truss optimization. *Eng. Comput.* **2019**, *37*, 641–662. [\[CrossRef\]](#)
27. Assimi, H.; Jamali, A.; Nariman-Zadeh, N. Multi-objective sizing and topology optimization of truss structures using genetic programming based on a new adaptive mutant operator. *Neural Comput. Appl.* **2019**, *31*, 5729–5749. [\[CrossRef\]](#)
28. Kumar, S.; Tejani, G.G.; Pholdee, N.; Bureerat, S. Multi-objective modified heat transfer search for truss optimization. *Eng. Comput.* **2020**, *37*, 3439–3454. [\[CrossRef\]](#)
29. Vargas, D.E.; Lemonge, A.C.; Barbosa, H.J.; Bernardino, H.S. Solving multi-objective structural optimization problems using GDE3 and NSGA-II with reference points. *Eng. Struct.* **2021**, *239*, 112187. [\[CrossRef\]](#)
30. Kaveh, A.; Laknejadi, K.; Alinejad, B. Performance-based multi-objective optimization of large steel structures. *Acta Mech.* **2012**, *223*, 355–369. [\[CrossRef\]](#)
31. Greiner, D.; Hajela, P. Truss topology optimization for mass and reliability considerations - Co-evolutionary multiobjective formulations. *Struct. Multidiscip. Optim.* **2012**, *45*, 589–613. [\[CrossRef\]](#)
32. Kaveh, A.; Farhoudi, N. A new optimization method: Dolphin echolocation. *Adv. Eng. Softw.* **2013**, *59*, 53–70. [\[CrossRef\]](#)
33. Kaveh, A.; Laknejadi, K. A new multi-swarm multi-objective optimization method for structural design. *Adv. Eng. Softw.* **2013**, *58*, 54–69. [\[CrossRef\]](#)
34. Pholdee, N.; Bureerat, S.; Jaroenapibal, P.; Radpukdee, T. Many-Objective Optimisation of Trusses Through Meta-Heuristics. In Proceedings of the International Symposium on Neural Networks, Sapporo, Japan, 21–26 June 2017; Springer: Berlin/Heidelberg, Germany, 2017; pp. 143–152.
35. Mokarram, V.; Banan, M.R. An improved multi-objective optimization approach for performance-based design of structures using nonlinear time-history analyses. *Appl. Soft Comput.* **2018**, *73*, 647–665. [\[CrossRef\]](#)
36. Mokarram, V.; Banan, M.R. A new PSO-based algorithm for multi-objective optimization with continuous and discrete design variables. *Struct. Multidiscip. Optim.* **2018**, *57*, 509–533. [\[CrossRef\]](#)
37. Techasen, T.; Wansasueb, K.; Panagant, N.; Pholdee, N.; Bureerat, S. Simultaneous topology, shape, and size optimization of trusses, taking account of uncertainties using multi-objective evolutionary algorithms. *Eng. Comput.* **2019**, *35*, 721–740. [\[CrossRef\]](#)
38. Carvalho, É.C.; Carvalho, J.P.G.; Bernardino, H.S.; Lemonge, A.C.; Hallak, P.H.; Vargas, D.E. Solving multi-objective truss structural optimization problems considering natural frequencies of vibration and automatic member grouping. *Evol. Intell.* **2024**, *17*, 653–678. [\[CrossRef\]](#)
39. Bathe, K.J. *Finite Element Procedures*; Prentice Hall, Pearson Education, Inc.: Hoboken, NJ, USA, 2006.
40. Deb, K.; Pratap, A.; Agarwal, S.; Meyarivan, T. A fast and elitist multiobjective genetic algorithm: NSGA-II. *IEEE Trans. Evol. Comput.* **2002**, *6*, 182–197. [\[CrossRef\]](#)
41. Kukkonen, S.; Lampinen, J. GDE3: The third Evolution Step of Generalized Differential Evolution. In Proceedings of the IEEE Congress on Evolutionary Computation (CEC 2005), Edinburgh, UK, 2–5 September 2005; IEEE: Piscataway, NJ, USA, 2005; pp. 443–450.
42. Zhang, Q.; Li, H. MOEA/D: A multiobjective evolutionary algorithm based on decomposition. *IEEE Trans. Evol. Comput.* **2007**, *11*, 712–731. [\[CrossRef\]](#)
43. Tušar, T.; Filipič, B. *DEMO (Differential Evolution for Multiobjective Optimization)*; Institut “Jožef Stefan”: Ljubljana, Slovenia, 2009.
44. Aittokoski, T.; Miettinen, K. Efficient evolutionary approach to approximate the Pareto-optimal set in multiobjective optimization, UPS-EMOA. *Optim. Methods Softw.* **2010**, *25*, 841–858. [\[CrossRef\]](#)
45. Pholdee, N.; Bureerat, S. Hybridisation of real-code population-based incremental learning and differential evolution for multiobjective design of trusses. *Inf. Sci.* **2013**, *223*, 136–152. [\[CrossRef\]](#)
46. Sadollah, A.; Eskandar, H.; Kim, J. Water cycle algorithm for solving constrained multi-objective optimization problems. *Appl. Soft Comput.* **2015**, *27*, 279–298. [\[CrossRef\]](#)
47. Mirjalili, S. Dragonfly algorithm: A new meta-heuristic optimization technique for solving single-objective, discrete, and multi-objective problems. *Neural Comput. Appl.* **2016**, *27*, 1053–1073. [\[CrossRef\]](#)
48. Mirjalili, S.; Saremi, S.; Mirjalili, S.; Coelho, L. Multi-objective grey wolf optimizer: A novel algorithm for multi-criterion optimization. *Expert Syst. Appl.* **2016**, *47*, 106–119. [\[CrossRef\]](#)
49. Mirjalili, S.; Jangir, P.; Saremi, S. Multi-objective ant lion optimizer: A multi-objective optimization algorithm for solving engineering problems. *Appl. Intell.* **2017**, *46*, 79–95. [\[CrossRef\]](#)
50. Mirjalili, S.; Gandomi, A.; Mirjalili, S.; Saremi, S.; Faris, H.; Mirjalili, S. Salp Swarm Algorithm: A bio-inspired optimizer for engineering design problems. *Adv. Eng. Softw.* **2017**, *114*, 163–191. [\[CrossRef\]](#)
51. Mirjalili, S.; Jangir, P.; Mirjalili, S.; Saremi, S.; Trivedi, I. Optimization of problems with multiple objectives using the multi-verse optimization algorithm. *Knowl.-Based Syst.* **2017**, *134*, 50–71. [\[CrossRef\]](#)
52. Mirjalili, S.; Mirjalili, S.; Saremi, S.; Faris, H.; Aljarah, I. Grasshopper optimization algorithm for multi-objective optimization problems. *Appl. Intell.* **2018**, *48*, 805–820. [\[CrossRef\]](#)

53. Tanabe, R.; Fukunaga, A. Success-history based parameter adaptation for differential evolution. In Proceedings of the IEEE Congress on Evolutionary Computation (CEC), Cancun, Mexico, 20–23 June 2013; pp. 71–78.
54. Mirjalili, S.; Lewis, A. The whale optimization algorithm. *Adv. Eng. Softw.* **2016**, *95*, 51–67. [[CrossRef](#)]
55. Bureerat, S.; Sriworamas, K. Population-based incremental learning for multiobjective optimisation. In *Soft Computing in Industrial Applications*; Springer: Berlin/Heidelberg, Germany, 2007; pp. 223–232.
56. Baluja, S. *Population-Based Incremental Learning: A Method for Integrating Genetic Search Based Function Optimization and Competitive Learning*; Technical Report; Carnegie Mellon University: Pittsburgh, PA, USA, 1994.
57. Zitzler, E.; Thiele, L. Multiobjective evolutionary algorithms: A comparative case study and the strength Pareto approach. *IEEE Trans. Evol. Comput.* **1999**, *3*, 257–271. [[CrossRef](#)]
58. Ishibuchi, H.; Masuda, H.; Nojima, Y. Sensitivity of Performance Evaluation Results by Inverted Generational Distance to Reference Points. In Proceedings of the 2016 IEEE Congress on Evolutionary Computation (CEC), Vancouver, BC, Canada, 24–29 July 2016; pp. 1107–1114.
59. Dolan, E.D.; Moré, J.J. Benchmarking optimization software with performance profiles. *Math. Program.* **2002**, *91*, 201–213. [[CrossRef](#)]
60. Barbosa, H.J.C.; Bernardino, H.S.; Barreto, A.M.S. Using performance profiles to analyze the results of the 2006 CEC constrained optimization competition. In Proceedings of the 2010 IEEE Congress on Evolutionary Computation (CEC), Barcelona, Spain, 18–23 July 2010; pp. 1–8.
61. Lemonge, A.C.; Barbosa, H.J. An adaptive penalty scheme for genetic algorithms in structural optimization. *Int. J. Numer. Methods Eng.* **2004**, *59*, 703–736. [[CrossRef](#)]

Disclaimer/Publisher’s Note: The statements, opinions and data contained in all publications are solely those of the individual author(s) and contributor(s) and not of MDPI and/or the editor(s). MDPI and/or the editor(s) disclaim responsibility for any injury to people or property resulting from any ideas, methods, instructions or products referred to in the content.